RGNZ/MGPB

Ore Genesis and Hydrothermal Evolution of the Cheshmeh-Hadi Stratabound (Manto-type) Copper Deposit in the Volcanic-Plutonic Belt North of the Doruneh Fault, East of the Sepid-Sarve copper deposit (NW Bardeskan, Central Iran): Evidence from Geology, Geochemistry, Fluid Inclusions, and Stable S and O Isotopes

Rudarsko-geološko-naftni zbornik
(The Mining-Geology-Petroleum Engineering Bulletin)
DOI: 10.17794/rgn.2026.3.11

Original scientific paper

Morteza Esform[1] ✉, Hasan Zamanian[2]* ✉, Alireza Zarasvandi[3] ✉, Alireza Almasi[1] ✉, Mahya Manouchehry Nia[1] ✉

[1] *Department of Geology, Faculty of Science, Lorestan University, Khorramabad, Iran.*
[2] *School of Geology, College of Science, University of Tehran, Tehran, 1417935840, Iran.*
[3] *Department of Geology, Faculty of Earth Sciences, Shahid Chamran University of Ahvaz, Ahvaz, Iran.*

Abstract

The Cheshmeh-Hadi copper deposit is part of an Eocene volcano-sedimentary sequence located in the southern Sabzevar Zone. The lithostratigraphic sequence, from oldest to youngest, comprises basalt, basaltic andesite, andesite and pyroxene andesite, conglomerate, limestone, siltstone, gypsiferous marl, and Pliocene conglomerate. The mineralized zone occurs within the conglomerate and at the contact between the conglomerate and andesite. The ore minerals consist of malachite-azurite, chalcocite, bornite, covellite and occasionally native copper. The associated hydrothermal fluids show moderate to high salinities, ranging from 3.09 to 13.39 wt.% NaCl equivalent, with homogenization temperatures between 89 and 387°C, indicating fluid mixing during ore formation. Chalcocite is rarely accompanied by quartz, suggesting low silica content in the ore-forming fluids. The $\delta^{34}S$ values of sulfide samples from the study deposit range from –24.1‰ to –2.6‰, while $\delta^{34}S$ values of hydrothermal H_2S range from –24.3‰ to –2.6‰. The $\delta^{18}O$ values of hydrothermal fluids associated with mineralization fall within the range of basaltic rocks, meteoric waters, and sedimentary rocks. Geochemical variations in major and trace elements suggest the involvement of continental crustal contamination in the magmatic evolution. The studied volcanic rocks fall within the calc-alkaline to shoshonitic fields, formed in a continental arc setting, and are derived from an enriched mantle source influenced by subduction-related fluids. These rocks are characterized by HREE depletion, moderate LREE enrichment, and a weak negative Eu anomaly. Based on the results, the Cheshmeh-Hadi deposit is classified as a stratabound copper sulfide deposit, formed in a volcano-sedimentary setting associated with a subduction-related magmatic arc environment.

Keywords:
Cheshmeh-Hadi, Stratabound Copper, Volcanic-Plutonic Belt, Stable Isotopes, Central Iran

1. Introduction

Numerous copper deposits and mineral occurrences are hosted in the uppermost Eocene volcanic sequences of Iran. Understanding these types of mineralization can offer new insight into the geology and copper resource potential of the region. Most stratabound (manto-type) copper deposits are hosted within stratigraphic sequences predominantly composed of andesitic to basaltic volcanic rocks. These sequences are associated with various geological eras, including the Mesozoic (in Chile and Iran), Proterozoic to Triassic (in North America), Late Silurian to Early Devonian (in China), and the Cenozoic (in Iran) (see **Figure 1**). To date, more than 30 significant manto-type copper deposits and numerous copper occurrences, ranging in age from the Cretaceous to the Eocene, have been identified in Iran. To date, more than 30 major Manto-type copper deposits and numerous copper occurrences ranging in age from Cretaceous to Eocene have been identified in Iran (e.g. the Veshnaveh deposit (**Fazeli, 2002**), Keshtmahaki (**Boveiri Konari et al., 2011**), Koshkoiye (**Abolipour et al., 2015**), the Vorezg-Qayen copper deposit (**Alizadeh et al., 2013**), the Abbas Abad copper deposit (**Maghfouri and Movahednia, 2015**), the Mari Cu(Ag) Manto copper deposit (**Maghfouri et al., 2017**), the Kahak Manto-Type copper deposit (**Kaboodi et al., 2019**), the Narbaghi deposit (**Fazli et al., 2021**), the Yamaghan Manto-Type Cu(Ag) deposit (**Jilba et al., 2021**) and the Madan Bozorg Cu deposits, Abbas Abad (**Salehi and Rasa, 2016**). Some of these deposits were historically exploited in ancient times – for example, the Veshnaveh deposit (**Fazeli, 2002**) and the Narbaghi deposit (**Fazli et al., 2021**) (see **Figure 1**). Some of these deposits, such as Veshnaveh and Eastern Narbaghi (in Qom and Saveh), were exploited during ancient times (see **Figure 1**).

* Corresponding author: Hasan Zamanian
e-mail address: hasanzamanian@ut.ac.ir
Received: 31 August 2025. Accepted: 2. December 2025.
Available online: 14 May 2026

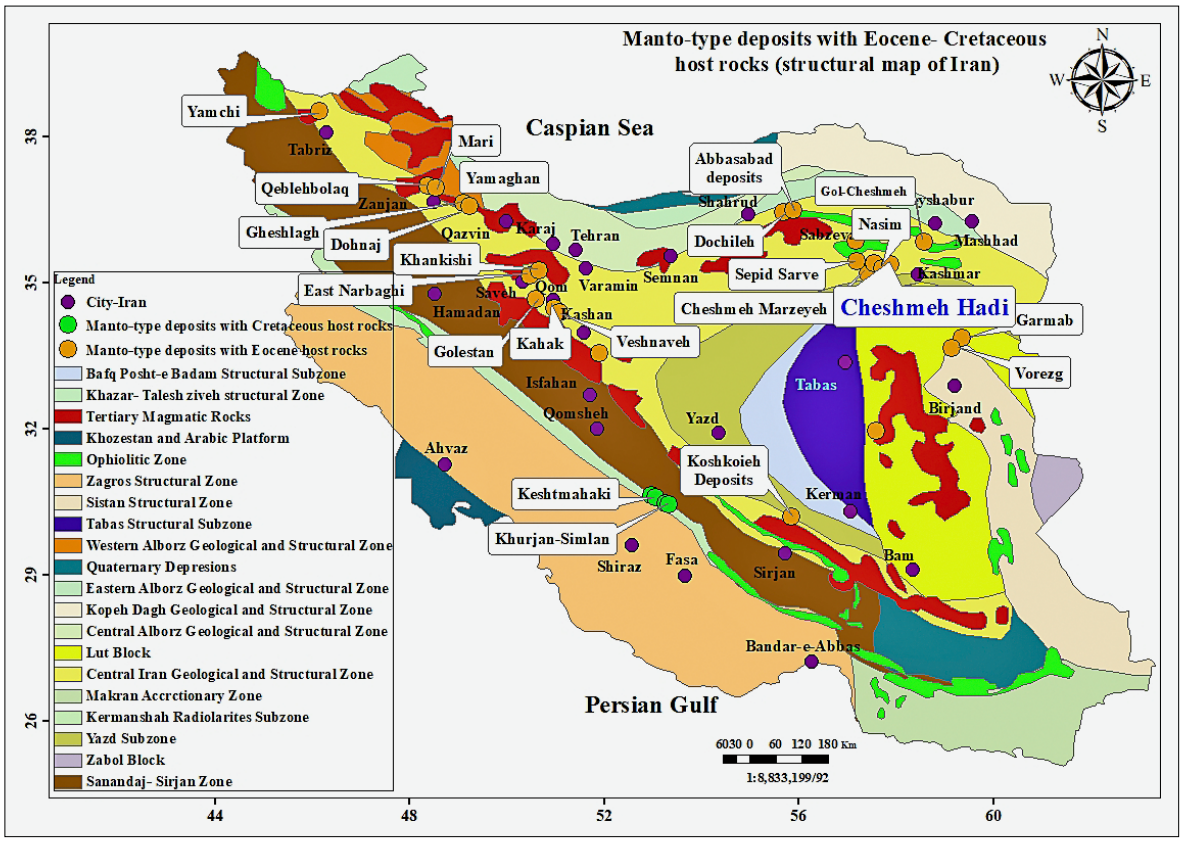

Figure 1. Location of Manto-type copper deposits in Iran and distribution map of these deposits based on the age of host rocks within the main tectonic zones of the country (**Aghanabati, 2004; Alavi, 1991**)

Manto-type deposits in Iran are typically associated with andesitic lava flows. The Eocene host rocks (Eocene volcano-sedimentary sequences) are the most common host lithologies for manto-type copper–silver deposits in Iran. These deposits are mainly concentrated within the Urumieh–Dokhtar Magmatic Arc (UDMA) (**Fazli et al., 2021**), the Alborz Magmatic Arc (AMA), the Sabzevar Zone, and the Lut Block. Approximately 85% of Iran's manto-type copper deposits occur within the UDMA, the Sabzevar Zone (north of the Doruneh Fault), and the AMA. Notable examples include the Abbasabad deposit in the Alborz range, Keshkuiyeh in the UDMA, and (e.g. Abri, Rahbari, and the Cheshmeh Marzeyeh Cu deposit (**Soltani, 2016**), the Bornaward plutonic complex (**Monazzami et al., 2018-2019**), the Baharieh copper deposit (**Rezaeihamid and Tale Fazel, 2019**), the Kal Abri copper deposit (**Jabari et al., 2016**), the Nasim copper deposit (**Ramezaniabbakhsh et al., 2023**), the Sharifabad copper deposit (**Ebrahimi et al., 2020**), Madan Bozorg (**Heidari, 2012**), Grik and Gukhab (**Taefi et al., 2014**), Golcheshmeh (**Entezari Harsini, 2017**), Cheshmeh-Hadi (**Rezapanah Khour, 2016**) in the southern Sabzevar Zone (north of the Doruneh Fault). The majority of the deposits are being actively explored. The Cheshmeh Marzeyeh copper deposit (**Soltani, 2016**), Kal Abri copper deposit (**Jabari et al., 2016**), the Nasim copper deposit (**Ramezaniabbakhsh et al., 2023**), Madan Bozorg (**Heidari, 2012**) and Cheshmeh-Hadi (**Rezapanah Khour, 2016**) deposits are presently mined (see **Figure 1**). The Cheshmeh-Hadi copper deposit is located in the southwest of Khorasan Razavi Province, approximately 46 km west of Bardeskan and 4 km from the village of Qaleh-Dahaneh (see **Figure 2**).

Volcano-sedimentary zones possess significant potential for the formation of Manto-type copper deposits. In the Cheshmeh-Hadi copper deposit area, Manto-type mineralization is associated with Eocene volcanic rocks and is controlled by specific geological horizons. The Doruneh sheet, located along the northern margin of Central Iran and the southern Sabzevar Zone, has acquired a distinctive geological position due to intense Cenozoic magmatic activity and the presence of the active Doruneh Fault. Consequently, a wide range of lithological units, from the Precambrian to the present, are exposed in this region.

The occurrence of vein-type mineralization within andesitic lava flows indicates that stratigraphic control plays a significant role in the deposition and formation of metals in Iran's Manto-type copper deposits. Thus, stratigraphic control is considered one of the major factors in ore formation. Moreover, both the lateral and vertical continuity of mineralization is strongly influenced by lithology, extensional fault systems, and the degree of rock fracturing.

This study characterizes the geological setting and mineralization style of the Cheshmeh-Hadi deposit, and

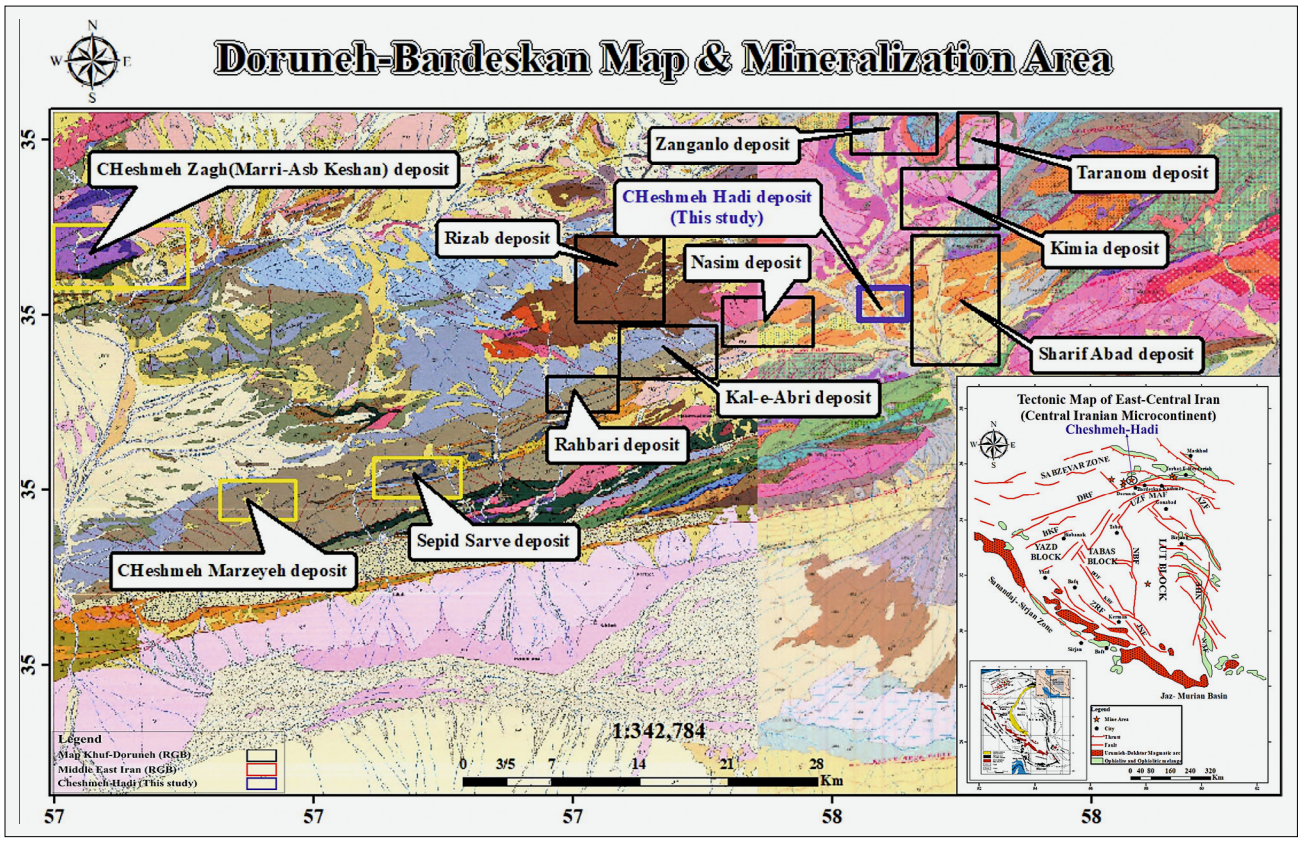

Figure 2. Location of the Cheshmeh-Hadi copper deposit in the southern part of the Sabzevar Zone (north of the Doruneh Fault)

proposes a large-scale mineralization model integrated with the tectono-magmatic evolution of the region, based on newly acquired field and analytical data. The results provide a refined exploration framework for identifying new manto-type copper targets in similar volcano-sedimentary settings, improve the understanding of ore-forming processes in the Sabzevar Zone, and offer practical guidelines for more effective exploration and resource development strategies in Iran's metallogenic provinces.

This research provides a comprehensive review of the Cheshmeh Hadi Manto-type copper deposit, highlighting its unique characteristics and formation processes. The findings contribute to a better understanding of metallogenic evolution in the southern part of the Sabzevar Zone (north of the Doruneh Fault) and emphasize the role of burial diagenesis in ore formation. The results are significant for mineral exploration and resource assessment in numerous Manto-type copper sulfide deposits distributed across the Sabzevar Zone, where the host rocks are predominantly volcanic sequences of Cretaceous to Tertiary age.

2. Materials and Methods

2.1. Geochemical analysis

As part of this study, and following an extensive literature review, a total of 134 samples were collected during fieldwork from intrusive and volcanic igneous units, as well as from mineralized veins and altered zones of the Cheshmeh-Hadi copper deposit. Sampling was conducted from the surface down to a depth of 56.2 meters to facilitate petrographic and lithological investigations. Corresponding thin sections were prepared for detailed analysis. Among these, 20 intrusive rock samples exhibiting minimal alteration were selected for whole-rock geochemical (lithochemical) analysis. Major elements in these samples were measured using X-ray fluorescence (XRF), following the processes of crushing, pulverizing, drying, homogenizing, powder preparation, pressing with boric acid, and finally fusion with lithium metaborate or tetraborate. For the analysis of rare earth elements (REEs) and trace elements, 0.2 grams of each sample was digested with diluted nitric acid and subsequently analyzed using inductively coupled plasma mass spectrometry (ICP-MS), based on ionization and separation of ions according to their mass-to-charge ratios. The analytical procedures were carried out at the Zar Azma Laboratory in Tehran. Multi-elemental analysis (56 elements) was performed using an Inductively Coupled Plasma Mass Spectrometer (ICP-MS) at Zar Azma Laboratory (Tehran, Iran). The analytical precision, evaluated through internal quality control and certified reference materials (NIST SRM 2709, 2710, and 2711), was approximately 3% for most elements and up to 10% for major elements. Calibration

and signal correction were conducted using multi-element calibration standards and internal standards (Sc, Ge, Rh, In, Bi), ensuring high analytical accuracy and reproducibility.

2.2. Fluid inclusions measurements

Five double-polished thin sections with a thickness of 80–100 μm were prepared from quartz and calcite (carbonate) veins and veinlets. Petrographic observations of fluid inclusion evidence were conducted, followed by microthermometric analyses on 40 fluid inclusions. These studies were carried out using a Linkam THMSG600 heating–freezing stage with a temperature range of −196°C to +600°C and a precision of ±1°C, at the Department of Geology, Tarbiat Modares University, Tehran. Temperature calibration was performed using Synflinc synthetic standards. During the freezing and heating procedures, the rates were controlled within the range of 1–10°C/min, before being decreased to 0.5–1°C/min in the vicinity of phase transition points. Salinities (wt.% NaCl equiv.) and densities (g/cm^3) of the aqueous (NaCl-H_2O) inclusions were determined using the computer program HOKIEFLINCS_H2O-NaCl Excel developed by **Steel-Maclnnis et al. (2012)** based on the final ice melting temperatures.

2.3. Stable isotope measurements

2.3.1. Oxygen isotope analysis

Two quartz and calcite samples were selected from the same vein locations where fluid inclusion samples were collected, for stable oxygen isotope ($\delta^{18}O$) analysis. The samples were first crushed to mesh 60 at the University of Tehran and then manually purified under a binocular microscope to achieve a purity of over 99%. After separation, the samples were powdered, sieved to remove contaminants, and rinsed with ethanol to ensure cleanliness. Isotopic analyses were performed at the Stable Isotope Research Center, Arak University, Iran. For $\delta^{18}O$ analysis in solid samples, high-temperature pyrolysis was conducted at 1450°C using an elemental analyzer, where all oxygen atoms in the molecular structure were converted to carbon monoxide (CO) gas in the presence of carbon black and glassy carbon. The resulting CO gas passed through a series of purification systems, including a water trap to remove moisture and a purge-and-trap column to eliminate CO impurities. After complete removal of interfering gases, the desorption column was heated to 150°C, and the purified CO gas was transferred through a secondary water trap into the isotope ratio mass spectrometer (IRMS). For calibration and calculation, the isotopic composition of the reference CO gas was determined by comparison with international or laboratory secondary standards. The mass ratio of 30.28 was measured to determine the $\delta^{18}O$ values. In this process, $\delta^{18}O$ is measured by converting the sample to CO gas via pyrolysis at 1450°C, followed by purification and subsequent analysis by IRMS, using the 30/28 mass ratio and calibrated against international standards. δ18O values exhibit a precision of 0.1‰ and are reported in reference to V-SMOW (Vienna Standard Mean Ocean Water, δ18O = 0, with uncertainties of 0.02‰; International Atomic Energy Agency, (2017).

2.3.2. Sulfur isotope analysis

Three representative chalcocite samples from mineralized veinlets were selected for sulfur isotope ($\delta^{34}S$) analysis. The samples were first powdered and sieved to obtain grain sizes between 0.1–0.5 mm. Clean mineral grains were handpicked under a binocular microscope to ensure purity. For isotopic analysis, the samples were combusted at 1150°C in an elemental analyzer, producing sulfur dioxide (SO_2) gas. The generated SO_2 gas was directed through a purification system consisting of a water trap to remove moisture and a purge-and-trap column to eliminate residual impurities. The adsorption column was subsequently heated to 220°C to release the accumulated SO_2 gas, which was then transferred into the isotope ratio mass spectrometer (IRMS). Within the IRMS, the sulfur isotopic composition was determined by measuring the mass ratio 66/64, corresponding to the $^{34}S/^{32}S$ ratio of the sample. To ensure the accuracy and reproducibility of the measurements, repeated calibrations were performed using the IAEA-S-4 international standard ($\delta^{34}S = +16.9 \pm 0.2$‰ VCDT) and a laboratory secondary standard ($\delta^{34}S = -6.3 \pm 0.2$‰ VCDT).

3. Geology

The Cheshmeh-Hadi copper deposit is part of an Eocene volcano-sedimentary sequence located in the southern Sabzevar Zone. This sequence comprises intermediate to mafic volcanic units (including porphyritic to megaporphyritic andesite, pyroxene andesite, and basalt), pyroclastic units (such as tuff and agglomerate), and a range of sedimentary rocks including fossiliferous limestone (with Nummulites, Plesiopoda, and Brachiopods), calcareous sandstones, detrital limestones, conglomerate, siltstone, shale, gypsiferous marl, and alluvial terraces (see **Figure 3**). The lithostratigraphic sequence, from oldest to youngest, comprises basalt, basaltic andesite, andesite and pyroxene andesite, conglomerate, limestone, siltstone, gypsiferous marl, and Pliocene conglomerate. The Cheshmeh Hadi copper deposit is located on the southern limb of an anticline. In this area, the youngest unit is a nummulitic limestone that overlies the conglomerate, cropping out along the outermost part of the anticline limb. The mineralized zone at Cheshmeh Hadi occurs within the conglomerate and at the contact between the conglomerate and andesite.

A distinctive feature of this region is the widespread development of Cretaceous volcanic–tuffaceous rocks

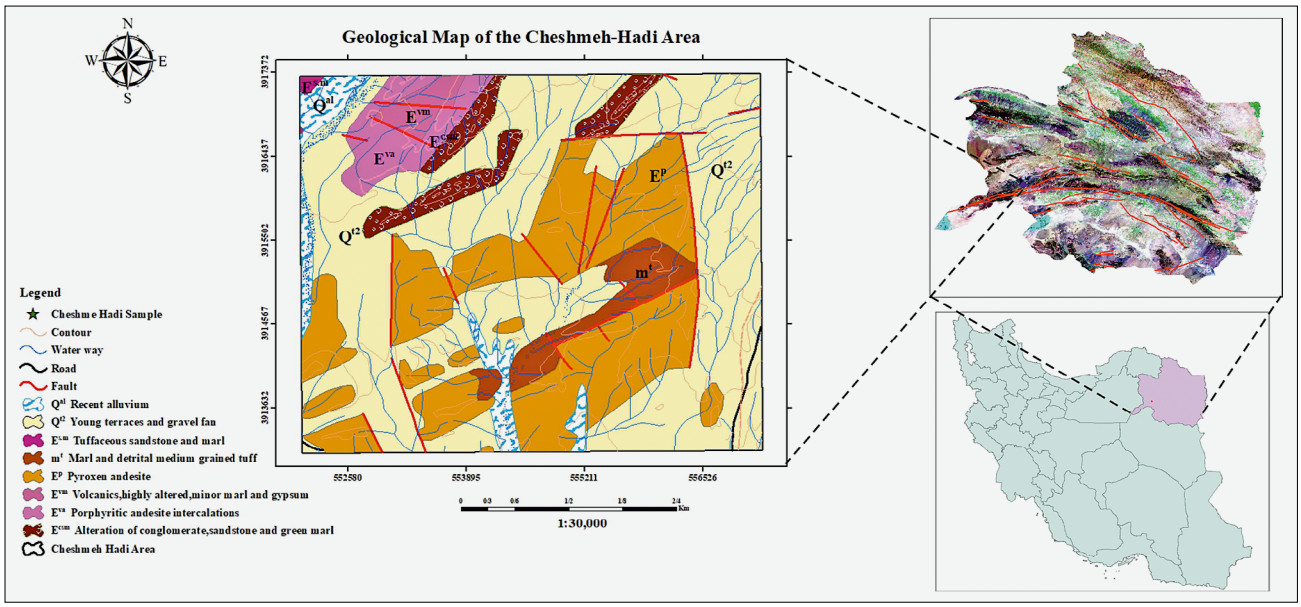

Figure 3. Detailed 1:1000 Geological Map of the Eastern Part of the Cheshmeh-Hadi Copper Deposit

and Eocene volcanic and pyroclastic units, reflecting significant volcanic activity in the area. In the central parts of the study area and within Middle Eocene sediments, a complex of volcanic and pyroclastic rocks is extensively exposed. This complex begins with volcanic rocks comprising andesite, pyroxene andesite, basaltic andesite, and basalt, typically dark green to black in colour. Most exposures display distinct bedding and banding. In some locations, agglomerates with green to red hues are interbedded within this volcanic sequence. Copper mineralization, mainly in the form of malachite, is observed along fractures within the andesitic rocks. Overlying the volcanic complex is a pyroclastic sequence consisting of alternating layers of agglomerate, tuff, lapilli tuff, and andesitic tuff with colours ranging from red to green (see **Figure 3**).

The Upper Eocene sediments are composed of alternating layers of sandstone, siltstone, silty marl, and thin-bedded limestone, typically light green to cream in colour. The Upper Eocene volcanic and pyroclastic rocks in the Cheshmeh-Hadi deposit area are subdivided into four distinct units. The first unit includes volcanic rocks such as andesite, porphyritic andesite, and pyroxene andesite, with green to dark gray colouration. Due to the alteration of phenocrysts in the andesites, an amygdaloidal texture has developed in many parts of these rocks (see **Figure 4A**). The vesicles are commonly filled with secondary minerals, such as calcite. Overlying this unit is a volcanic complex consisting of basalt and basaltic andesite with black colouration. Above this volcanic–pyroclastic complex, Oligo–Miocene sedimentary deposits are present. Therefore, this volcanic assemblage may be regarded as representing the final phase of Eocene volcanic activity. The main volcanic rocks of the area exhibit gentle morphology and are locally vesicular, with vesicles typically filled by calcite, silica, and occasionally zeolite.

3.1. Conglomerate

The highest stratigraphic unit in the Cheshmeh Hadi deposit area is the Pliocene–Pleistocene conglomerate, which represents the thickest and most extensive sedimentary unit at the uppermost horizon. Its characteristic features include a gray to reddish-brown colouration, lack of induration, weak cementation, polymictic clast composition, presence of clay–iron oxide cement with very low strength, and the development of relatively subdued topography. The conglomerate associated with mineralization in the Cheshmeh Hadi copper deposit is composed of rounded clasts with an average size of 3–4 cm, predominantly derived from volcanic rocks such as andesite (see **Figure 4A**), pyroxene andesite (see **Figure 4B**), trachyte, trachyandesite, dacite, and andesitic tuff. In addition, clasts of intrusive units (monzonite, diorite, and pyroxene diorite) as well as subvolcanic rocks (porphyritic diorite, porphyritic monzodiorite, and porphyritic monzonite) are also observed. This conglomerate contains volcanic cement in proximity to volcanic units (andesite), whereas toward the limestone contact, the clast size decreases and the cement becomes carbonate in composition, reflecting deposition in a marine setting alongside the limestone unit. Furthermore, in conglomerates adjacent to limestone, sedimentary clasts such as shale are also present. Mineralization occurs mainly as chalcocite within the conglomerate, where effective porosity is available, and occurs sporadically within andesite and limestone as well. The timing of mineralization postdates the formation of the conglomerate and the limestone in the area. No sedimentary units are developed within the volcanic sequence, and the observed

structures and textures indicate a non-marine environment. The volcanic cement at the base of the conglomerate contains magnetite. Since the volcanic rocks themselves contain approximately 3–5% magnetite, the presence of magnetite in the conglomerate cement does not indicate paragenesis with chalcocite; rather, as noted, the ore-forming fluid responsible for chalcocite was iron-deficient at the time of mineralization. The magnetite present is attributed to the erosion and redeposition of volcanic rock fragments during conglomerate formation.

3.2. Andesitic and basaltic andesite

The Eocene andesitic and basaltic andesite volcanic units show mineralogical, textural, and lithological diversity. These lava flows are conformable and parallel to adjacent units. Fresh andesites are dark gray, weathered to grayish-brown, with some areas stained reddish by iron oxides. Hand samples reveal porphyritic, megaporphyritic, vesicular, amygdaloidal, and flow textures, featuring phenocrysts of plagioclase, pyroxene, and opaque minerals (see **Figure 4C**). Vesicles are often filled with secondary silica, calcite, and chlorite minerals, giving amygdaloidal and vesicular textures.

3.3. Pyroxene andesite

The pyroxene andesite unit appears as low-relief hills with a light gray colour and displays porphyritic and amygdaloidal textures (see **Figure 4D**). Hand specimens contain rounded pyroxene crystals and coarse plagioclase crystals (27–36%). Secondary minerals like chlorite and calcite are present as veinlets and vesicle-fillings, with carbonate veins measuring 1.5–2.5 mm clearly visible (see **Figure 4E**). Phenocrysts constitute approximately half of the rock's volume. Plagioclase makes up about 75–80% of the phenocrysts, pyroxene 15–20%, and alkali feldspar 2–3%. The plagioclase phenocrysts range in size from 1 to 2 mm, pyroxene from 300 micrometers to 2 mm, and alkali feldspar phenocrysts are approximately 200–300 micrometers in size (see **Figure 4E**). Some plagioclase crystals exhibit oscillatory zoning (see **Figure 4E**), indicative of intermediate composition (andesine). Plagioclase phenocrysts also display sieve texture. Pyroxene frequently exhibits oxidized rims, suggesting that the rock erupted at the Earth's surface (see **Figure 4F**). The groundmass consists of fine-grained feldspar crystals and volcanic glass (see **Figure 4G**). The feldspars are unaltered, while the pyroxene is partially altered to secondary iron oxides (iddingsite) (see **Figure 4H**). The glomeroporphyritic texture is observed in the rock due to the aggregation of phenocrysts. Minor amounts of alkali feldspar phenocrysts, measuring approximately 200 micrometers, are also present. The groundmass consists of feldspar microlites and iron oxides (see **Figure 4H**). Scattered carbonate fragments are observed in the rock, resulting from weak carbonation alteration (see **Figure 4I**). The mineral celadonite is green and similar in appearance to malachite (see **Figure 4K**). Scattered green grains and crystals (often associated with carbonate minerals) are observed in the rock (see **Figure 4I**).

3.4. Marl and siltstone

The E^{csm} unit consists of thinly bedded marl and siltstone layers, ranging from light gray to cream, overlying the fossiliferous limestone. It forms hilly terrain, with greater thickness and lateral extent in the western sector compared to the east. This unit is conformably overlain by a red marl layer. Notably, limestone beds analogous to E^{csm} occur within the northern part of the western sector, hosting malachite mineralization, and have been structurally emplaced into the marl via thrust faulting.

The E^{vm} unit includes marls with transparent gypsum layers, gray to white in colour, present in both eastern and western sectors. It locally overlies older units discontinuously, with wider distribution in the east and beyond the study area. The unit hosts multiple high-quality gypsum layers currently under extraction, displaying rugged topography and limited thickness.

3.5. Alteration

Magmatic and hydrothermal fluids derived from volcanic eruptions generally cause very weak alteration within the host rock units, mostly resulting in chloritic and iron oxide alterations (see **Figure 4I**). Chlorite can form either through alteration of mafic minerals present in the rock or by the introduction of iron and magnesium via hydrothermal fluids (see **Figure 4N**). Zeolitic alteration is observed locally within the Cheshmeh-Hadi copper deposit; the formation of zeolites in intermediate to basic rocks is related to hydrothermal alteration (see **Figure 4L**), low-grade metamorphism, and alteration by meteoric waters. Iron oxide staining, chloritization, and iddingsitization occur with weak to moderate intensity in andesitic units, while carbonate and clay alteration are weakly developed (see **Figure 4M**). Iron oxide alteration is likely due to the transformation of pyrite to goethite–hematite (see **Figure 4M**), which facilitates the release of sulfur and its combination with sulfide ions, promoting the formation of sulfide minerals, such as chalcocite and digenite. Secondary processes have transformed copper oxide minerals like malachite from primary sulfides. Alteration in the Cheshmeh-Hadi deposit, similar to much of the northwest Bardeskan region, can be divided into two stages: pre-mineralization and syn-mineralization. Pre-mineralization alteration includes celadonite, carbonate, silicification, and propylitic (epidote and chlorite) assemblages (see **Figure 4N**), whereas syn-mineralization alteration mainly consists of carbonate, zeolite, calcite, minor chlorite, and subordinate argillic alteration. The pre-mineralization alteration corresponds to regional propylitic alteration, while syn-mineralization alteration is characterized by localized

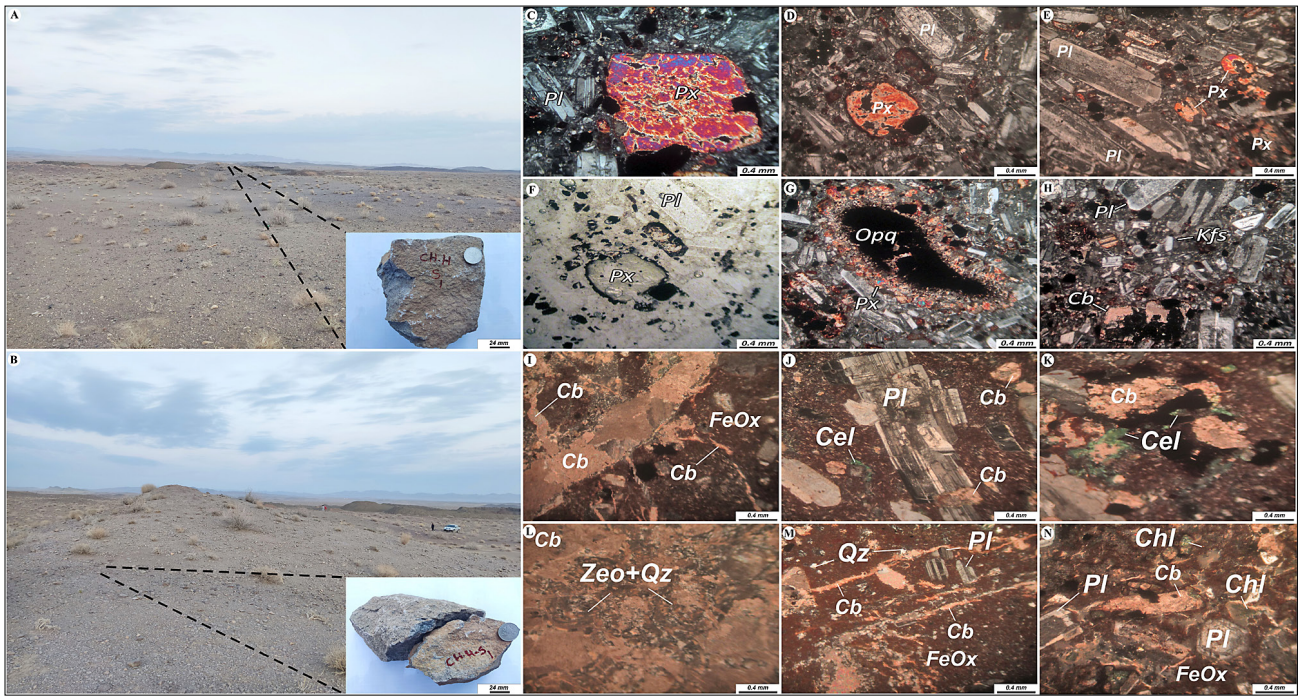

Figure 4: Overview of the Cheshmeh-Hadi copper deposit area: (**A**) Andesite unit. (**B**) Pyroxen andesite unit. (**C**) Pyroxene and plagioclase phenocrysts. (**D**) Pyroxene and plagioclase phenocrysts. (**E**) Pyroxene and plagioclase phenocrysts. (**F**) Pyroxene crystal with oxidized margins, indicating volcanic eruption at the Earth's surface. (**G**) Aggregate of opaque minerals replacing the margins of pyroxene. (**H**) Alkali feldspar occurring as a minor constituent in the rock. (**I**) Alkali feldspar together with plagioclase in basaltic andesite. (**J**) Plagioclase phenocryst and carbonate fragments within the rock. (**K**) Chlorite mineral associated with celadonite (green in colour) and carbonate in andesite. (**L**) Plagioclase phenocryst accompanied by quartz crystals. (**M**) Plagioclase phenocryst with carbonate veinlets within an iron oxide-rich matrix. (**N**) Plagioclase phenocryst showing a sieve texture in a groundmass composed of iron oxides and carbonate minerals, with chlorite occurring as interlocking fragments, while carbonate veinlets cut across the rock matrix. (Px: pyroxene, Cel: Celadonite, Pl: plagioclase, Chl: Chlorite, Qz: Quartz, Zeo: Zeolite, Opq: Opaque, Cb: Carbonates, Kfs: K-feldspar, Feo_x: Fe-oxides) (Mineral abbreviations are taken from **Warr, 2021**).

carbonate, calcite, zeolite, and minor argillic alteration. Hydrothermal alteration in the Cheshmeh Hadi copper deposit can be divided into two groups: pre-conglomerate alterations and post-conglomerate alterations (the latter being synchronous with and related to mineralization). Pre-conglomerate alterations include those observed in volcanic rock fragments – zeolitization, kaolinitization, carbonatization, and celadonitization – as well as alterations in subvolcanic bodies such as monzonite and porphyritic diorite (in the form of dikes), which include propylitic alteration (epidote and occasionally chlorite) and silicification. Zeolitization, dominated by natrolite, is most common in megaporphyritic andesites and porphyritic trachyandesites, formed through multiple stages. In many cases, cavities between grains and large plagioclase phenocrysts are filled with radial natrolite zeolites. This alteration unit represents the basal part of the stratigraphic sequence and its fragments are observed within the conglomerate along with other volcanic rock clasts. Zeolitization is especially prominent in the northern part of the Cheshmeh Hadi deposit. Chloritization, and locally iddingsitization, occurs in porphyritic andesites, pyroxene andesites, and, to a lesser extent, in basalts and basaltic andesites outcropping in the western and northwestern parts of the area. Hydrothermal fluids altered mafic minerals such as pyroxene and olivine to chlorite, forming chloritic alteration, while the breakdown of olivine produced iddingsite. These alterations impart a dark green colouration to the affected rocks. Since these processes are observed in andesite, basaltic andesite, and pyroxene andesite units that constitute the clasts of the conglomerate, the same alteration features can clearly be identified within the conglomerate clasts as well.

4. Results and discussion

4.1. Structural Geology

In general, several fault systems can be recognized in the study area, including E–W and N–S trending faults, as well as dextral strike-slip faults trending NW–SE and NE–SW, which are the most dominant fault types in the Cheshmeh-Hadi copper deposit. These faults have, in some areas, displaced the mineralized zones. In the easternmost part of the area, overturned limestone units are observed in certain locations, indicating intense tectonic activity in this part of the deposit. In this section, several

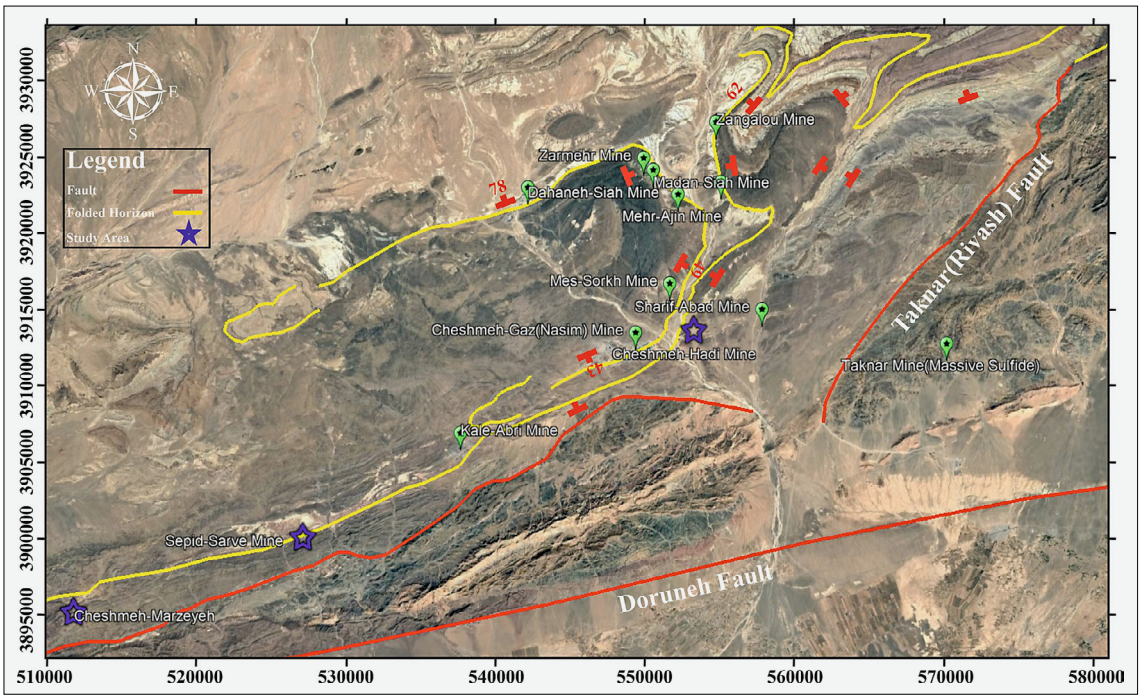

Figure 5. View of the fault and Folded Horizon systems present in the eastern part of the Cheshmeh-Hadi copper deposit

strike-slip faults with approximately NW–SE orientation have disrupted the limestone layers and displaced copper mineralization that occurs at the contact between limestone and volcanic units (see **Figure 5**).

4.2. Economic Geology

4.2.1. Mineralization

Copper mineralization in the Cheshmeh-Hadi deposit has developed along the contact zones between pyroclastic and volcanic units and overlying carbonate sequences (including marly, fossiliferous, and clastic limestones). Mineralization is predominantly located below the carbonate horizon and within the upper portions of volcanic and volcaniclastic units composed of conglomerate, andesite (see **Figure 6A**), and agglomerate (see **Figure 6B**). In some localities, oxide copper mineralization occurs at the upper boundary of the limestone in contact with shale and marl. The mineralized zones vary in thickness and dip steeply to nearly vertical. The ore minerals include malachite (see **Figure 6B**), azurite, chalcocite (see **Figure 6C**), digenite, cuprite, covellite, and locally native copper. Mineralization occurs as veinlets (see **Figure 6D**), cavity-fillings, disseminations (see **Figure 6E**) and impregnation textures. The host rocks for veinlet-style mineralization mainly consist of andesitic and pyroclastic rocks, with limestone playing a lesser role. The high porosity and permeability of conglomerates provided favourable pathways for hydrothermal fluids or metamorphic-derived brines, facilitating mineral precipitation as open-space fillings and disseminated textures. These conglomerates commonly contain fragments of volcanic and agglomeratic rocks. The Cheshmeh-Hadi deposit is situated at the southeastern termination of the Khaf–Kashmar–Bardeskan magmatic belt, within the Sabzevar subzone. The dominant lithology comprises Eocene to Miocene volcano-sedimentary sequences. Intense compressional tectonics have produced a series of anticlines and synclines, with the mineralized zones hosted along the limbs of these structures. The high permeability of the conglomerates promoted fluid circulation and metal precipitation. The ore mineral assemblage includes chalcocite, minor chalcopyrite and bornite, covellite, pyrite, malachite (see **Figure 6I**), and chrysocolla. Chalcocite, bornite (see **Figure 6F**), and pyrite are interpreted as primary sulfides that were later altered to secondary minerals such as malachite, covellite (see **Figure 6G**), and iron hydroxides during supergene enrichment (see **Figure 6H**). The dominant alteration types include chloritic, carbonatic, and zeolitic alterations, with limited zones of argillic alteration. Chalcocite is considered the most important primary copper mineral in manto-type deposits, characterized by high copper content and the absence of iron (**Movahednia et al., 2022**). In contrast, chalcopyrite, the principal copper mineral in porphyry, VMS, and other systems, contains less copper and a higher proportion of iron. The presence of chalcocite without iron-bearing gangue minerals and the absence of quartz indicates that the mineralizing fluids were copper-rich, iron-poor, and silica-deficient, suggesting highly reducing conditions (**Rameza-niabbakhsh et al., 2023**). The lack of epidote – a mineral associated with oxidizing conditions and high iron – supports this interpretation. Although the volcanic host rocks contain up to 5% primary magnetite (see **Fig-**

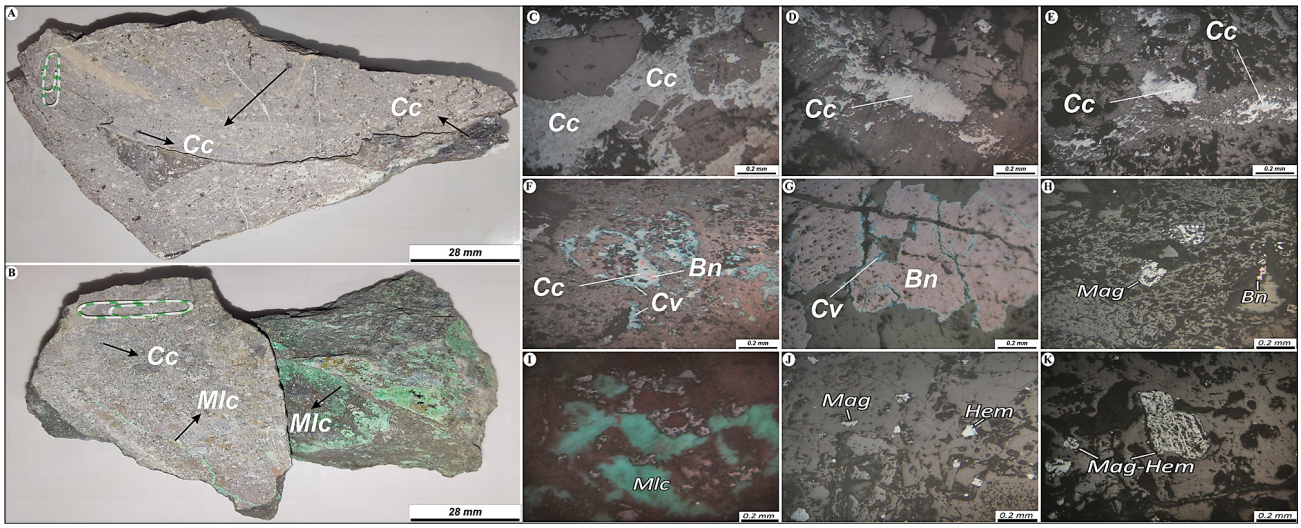

Figure 6. (**A**) Hand specimen showing oxide and sulfide copper mineralization. (**B**) Hand specimen with oxide and sulfide copper mineralization. (**C**) Section of a thick chalcocite vein cut by a second generation of chalcocite veinlets. (**D**) Thin chalcocite veinlets accompanied by fine disseminated grains. (**E**) Chalcocite occurring as disseminated crystalline grains. (**F-G**) Bornite altered to covellite and chalcocite along grain boundaries and fractures. (**H**) Magnetite and disseminated bornite grains. (**I**) Malachite vein under polarized light, appearing green in colour. (**J**) Magnetite crystals, some of which are partially replaced by hematite. (**K**) Hematitized magnetite minerals. (Cc: Chalcocite, Cv: Covellite, Bn: Bornite, Mag: Magnetite, Mlc: Malachite, Hem: Hematite) (Mineral abbreviations are taken from **Warr, 2021**).

ure 6J), there is no evidence of iron-rich mineralization, such as widespread chalcopyrite or pyrite in the deposit, implying that the volcanic rocks are unlikely to be the metal source (see **Figure 6K**). These rocks also show no significant alteration. Likewise, if intrusive bodies were the metal source, the hydrothermal fluids would be expected to be rich in silica, iron, and aluminum. However, the absence of quartz associated with chalcocite suggests otherwise.

In recent decades, several studies have emphasized the role of framboidal pyrite and bitumen in the genesis of mantle-type copper deposits (**Zentilli et al., 1997; Wilson, 2000; Herazo et al., 2020**). Framboidal pyrite is a common pre-ore reducing agent in Iranian stratabound copper deposits (**Movahednia et al., 2022**). For example, in the Keshkuiyeh deposit, the highest copper grades are found in veins and zones closely associated with pyrobitumen and framboidal pyrite. These pyrite textures are widespread and typically occur as fine-grained aggregates in close proximity to copper mineralization, suggesting their critical role in ore formation. In Iranian mantle-type deposits, the pre-ore mineral assemblage typically includes framboidal pyrite and pervasive propylitic alteration affecting andesitic host rocks (see **Figures 7A, B and C**). This assemblage, reported from other stratabound deposits as well, is often interpreted as a product of early diagenesis or pre-hydrothermal processes (**Maghfouri et al., 2017**). Framboidal pyrite formed during early diagenesis may be partially replaced by Cu-(Fe) sulphides, such as chalcocite and bornite, during burial diagenesis (see **Figure 7D**). The presence of zeolite minerals during later burial suggests continued diagenetic evolution (**Maghfouri et al., 2017**). These findings indicate that metal-bearing hydrothermal fluids may have interacted with pre-existing pyrite, which acted as a reducing agent, triggering the precipitation of copper sulfides (**Dissanayake, 1993; Herazo et al., 2020**). Such pyrite replacement processes have also been proposed for stratabound copper deposits in central Chile (**Zentilli & Wilson, 1999; Merinero et al., 2019**).

The ore minerals primarily formed in the cavities and fractures of the host rock, as well as in the micro-fractures and voids of minerals such as pyroxene, plagioclase, and hornblende. The primary hypogene minerals in the Cheshmeh Hadi deposit include chalcopyrite, pyrite, chalcocite (see **Figure 7B**), and hematite. Chalcocite is the most abundant copper sulfide mineral, occurring disseminated and in veinlets within fractures and voids of the host rock and minerals, and in some cases, it has altered to covellite (see **Figure 7I**). Calcite veinlets, and to a lesser extent quartz veinlets, are more widespread at this stage, and minerals like chalcocite commonly occur within these veinlets. Pyrite and chalcocite are present in very small amounts, typically less than 60 microns, and are dispersed in the host rock cavities. Hematite forms as a replacement of magnetite nodules in the cavities; the magnetite crystals belong to the andesitic unit and are unrelated to copper mineralization (see **Figure 7K**). Upon exposure to surface conditions, the copper sulfide minerals undergo oxidation, leading to the formation of secondary supergene minerals such as malachite, azurite (see **Figure 7A**), and covellite. Malachite, the most abundant supergene mineral (see **Figure 7E**), and azurite generally form as replacements of primary copper sulfides like chalcocite, filling fractures and

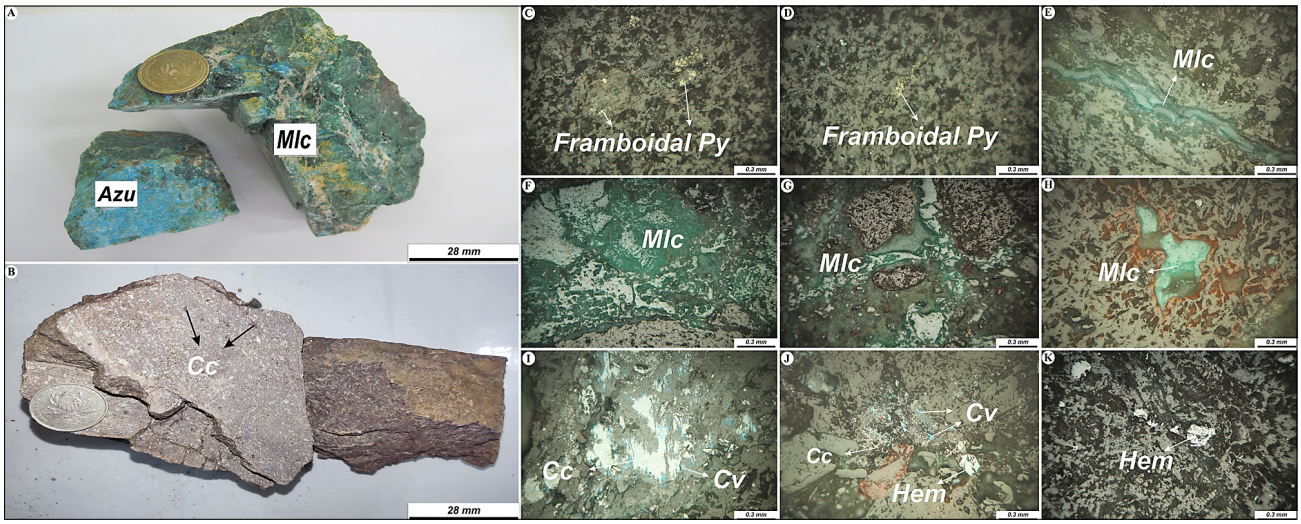

Figure 7. (**A**) Occurrence of chalcocite with disseminated texture, filling interstitial spaces within the rock, accompanied by malachite with a cavity-filling habit. (**B**) Malachite filling voids and grain boundaries, together with chalcocite occurring as irregular fragments dispersed throughout the rock. (**C-D**) Pyrite occurring as fine grains with spherical and framboidal (clustered) textures, disseminated in the host rock. (**E**) Chalcocite as fine- to medium-grained fragments, scattered within the rock and associated with malachite; in some cases, chalcocite is replaced by covellite. (**F-G-H**) Malachite as the only copper-bearing mineral filling fractures in a vein-like manner, accompanied by hematite as irregular fragments disseminated in the rock, apparently formed contemporaneously with the host andesitic rocks. (**I-J-K**) Hematite occurs as scattered grains, chalcocite is present as aggregates ranging from fine- to relatively coarse-grained (mostly associated with covellite), and malachite is distributed as smaller dispersed fragments within the rock. (Cc: Chalcocite, Cv: Covellite, Azu: Azurite, Py: Pyrite, Mlc: Malachite, Hem: Hematite) (Mineral abbreviations are taken from **Warr, 2021**).

cavities (see **Figure 7F**). Covellite is present in very minor amounts and forms from the alteration of chalcocite (see **Figure 7I**). Goethite results from the alteration of iron oxides such as hematite and magnetite (see **Figure 7J**). Based on microscopic studies of texture, structure, and mineralogy, the mineralization can be divided into hypogene and supergene stages. During the hypogene stage, pyrite, chalcocite, and chalcopyrite formed along with minor quartz and calcite. Hematite, resulting from the alteration of magnetite, formed in the late hypogene stage (see **Figure 7G**). In the supergene stage, upon exposure to surface conditions, secondary minerals such as malachite (see **Figure 7H**), azurite, and covellite formed from the oxidation of copper sulfides, while goethite formed from the oxidation of iron-bearing minerals such as hematite and magnetite (see **Figure 7K**).

4.2.2. Paragenesis

Given that chalcocite is the hallmark mineral of the Manto type and is dominant within the Cheshmeh-Hadi copper deposit, lesser amounts of bornite, pyrite, digenite, magnetite, and hematite are sporadically observed as primary metallic minerals. Secondary minerals including malachite, azurite, secondary chalcocite, covellite, and hematite have formed in various parts of the Cheshmeh-Hadi deposit (see **Figure 8**). These minerals exhibit textures such as disseminated grains, cavity-filling (amygdaloidal), martitization, replacement, and skeletal structures. Most of these minerals occur as veinlets of varying lengths and thicknesses, as well as disseminated grains.

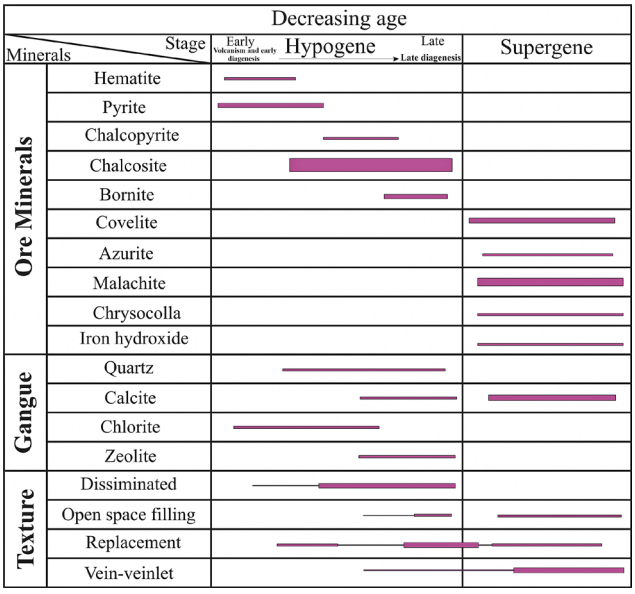

Figure 8. Paragenesis diagram of selected minerals in the Cheshmeh-Hadi copper deposit

4.3. Fluid Inclusions

Fluid inclusions are commonly used to determine temperature, solute type, and salinity of mineralizing solutions in various deposits. In the Cheshmeh-Hadi copper deposit, fine-crystalline calcite is the most abundant and significant mineral associated with the main mineralizing fluid. The studied fluid inclusions occur as mono-phase (liquid, L; vapor, V), and two-phase liquid-rich (see **Fig-**

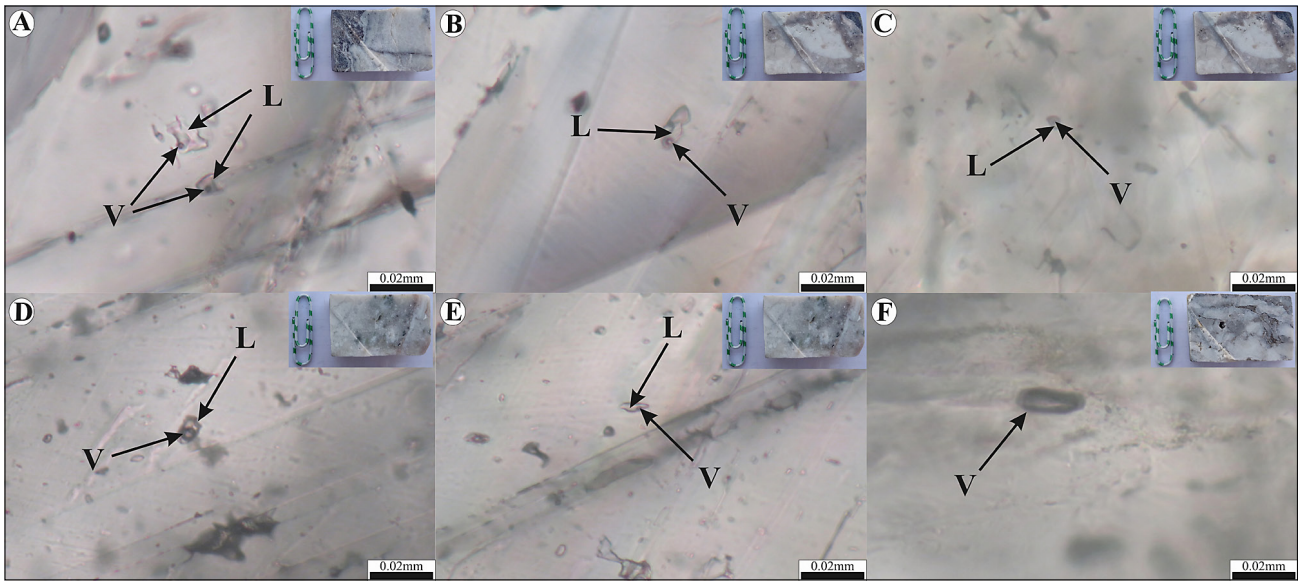

Figure 9. (**A**) Two-phase fluid inclusion enriched in liquid (L+V). (**B**) Two-phase fluid inclusion enriched in vapour (V+L). (**C**) Two-phase fluid inclusions enriched in liquid phase (L+V). (**D**) Mono-phase gaseous fluid inclusion. (**E**) Mono-phase gaseous fluid inclusions. (**F**) Mono-phase gaseous fluid inclusions.

Table 1. Microthermometric data of fluid inclusions in the Cheshmeh-Hadi copper deposit

Sample N.	Mineralization Type	Mineral	phase	Tutec (°C)	Tice(°C)	salinity	Th V-L (°C)	Th L-V (°C)	THT (°C)
S08	Mlc+Az+Cal	Calcite	L+V	-36.5	(-2.2)-(-5.6)	3.36-9.07	133-212		133-212
S11	Cct+Cal	Calcite	L+V	-41	(-2.8)-(9.1)	4.46-12.61	174-332		174-332
S11	Cct+Cal	Calcite	V+L		(-7.7)-(-8.18)	11.21-11.61		263-343	263-343
S13A	Mlc+Az+Cal	Calcite	L+V	-49.7	(-1.9)-(-9.3)	3.09-13.19	89-387		89-387
S17A	Cct+Bn+Ccp+Mag+Qtz	Quartz	L+V	-39.5	(-1.8)-(-9.4)	3.38-13.39	102-235		102-235
S17A	Cct+Bn+Ccp+Mag+Qtz	Quartz	L+V+S		-7.9	11.53	279		279
S14B	Mlc+Az+Cal	Calcite	L+V	-37.1	(-2.1)-(-5.2)	3.37-7.84	147-273		147-273
S14B	Mlc+Az+Cal	Calcite	V+L		(-5.5)-(-5.6)	8.78-8.99		282-302	282-302

ures 9A, C) plus vapour-rich (L+V) types (see **Figure 9B**), mostly irregular, rectangular, spherical, or elliptical in shape and dark in colour. mono-phase vapor inclusions range from 2 to 10 microns, predominantly irregular in shape. In liquid–vapor (L+V) inclusions where the liquid phase occupies a larger volume, the vapor (gas) phase transforms into the dominant liquid phase upon homogenization. Conversely, in vapour–liquid (V+L) inclusions where the vapour occupies a greater volume, the liquid phase transforms into the dominant vapour phase during homogenization. The homogenization temperature to the liquid phase (TH_{V+L}) represents the temperature at which the vapour phase becomes completely homogenized into the liquid phase. The homogenization temperature to the vapour phase (TH_{L+V}) denotes the temperature at which the liquid phase becomes homogenized into the vapour phase. The temperature of the first ice melting (Tu) indicates the closure of the system. The halite melting temperature (THH) reflects the salinity of the fluid, which can be calculated from the measured value. The final ice melting temperature (THT) also represents fluid salinity in the absence of a halite phase; it is measured as a negative value but is conventionally reported as a positive number in calculations. In the studied samples, mono-phase gas-rich inclusions are the most common type, ranging in size from 2 to 15 microns and mostly occurring in irregular and oval shapes. Two-phase, liquid-rich inclusions are very rare, with the vapour phase making up approximately 10–35% of the total inclusion volume. Their sizes range from 5 to 15 microns, and they are mostly irregular in shape. Two-phase, vapour-rich inclusions are around 14 microns in size, with shapes varying from spherical to flattened. Overall, fluid inclusion sizes in the deposit range from a few microns upward. Mono-phase vapour inclusions occur sporadically and individually within the host (see **Figures 9D, E,** and **F**), while two-phase, liquid-rich inclusions are mostly isolated (see **Figures 9A** and **C**) (see **Table 1**).

The first melting temperature is directly related to the salt composition of the hydrothermal fluid (**Shepherd et**

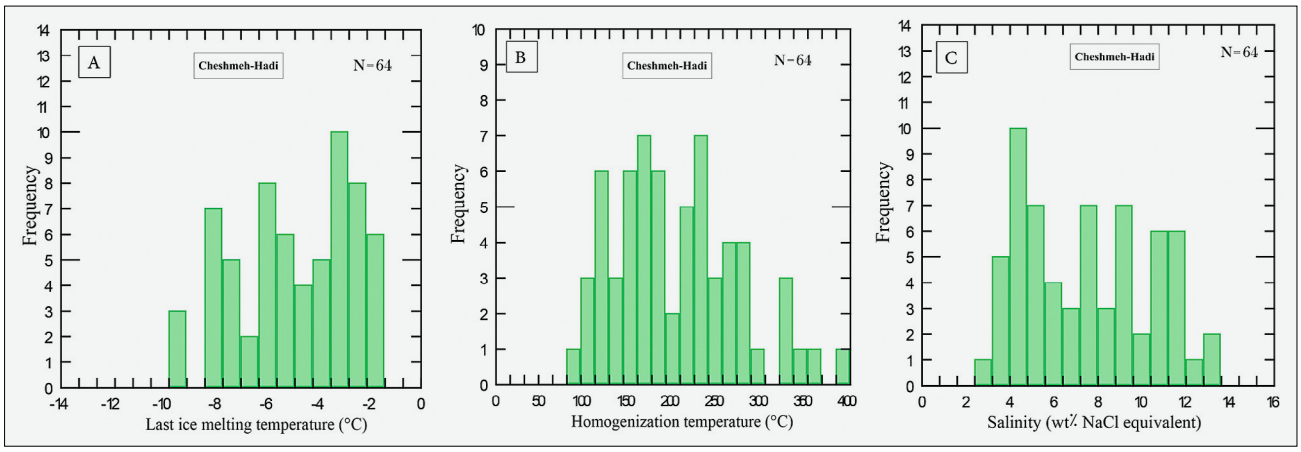

Figure 10. Histograms of fluid inclusion data: (**A**) Final ice-melting temperature. (**B**) Homogenization temperature. (**C**) Salinity

al., 1985) (see **Figure 10A**). Homogenization temperatures (Th) of vapour + liquid (L+V) inclusions range from 89 to 387°C, averaging 194.75°C, while for liquid + vapour (V+L) inclusions Th ranges from 263 to 343°C, averaging 304.6°C (see **Figure 10B**). Salinity varies from 3.08 to 13.38 wt.% NaCl equiv., with an average of 7.56 wt.% (see **Figure 10C**).

Based on fluid inclusion studies, the formation temperature of the Cheshmeh-Hadi copper deposit ranged between 90 and 386°C, originating from a solution containing 3.09 to 13.39 wt.% NaCl. The final ice melting temperatures of fluid inclusions vary from –6.9 to –8.18°C. Salinity, a key factor influencing fluid density, was evaluated using homogenization temperature versus salinity plots for mineralizing inclusions from Cheshmeh-Hadi (**Bodnar, 1983**). Fluid densities vary between 0.7 and 1 g/cm³ (see **Figure 11**). A decrease in homogenization temperature from 387 to 89°C corresponds to a density increase from below 0.7 to 1 g/cm³, resulting in reduced fluid velocity and enhanced mineral precipitation.

The increase in salinity in fluid inclusions over the 89 to 387°C range is accompanied by rising density. This process is linked to boiling phenomena whereby, due to cooling or pressure drop, fluids evolve toward a denser, more saline phase compared to the initial fluid. However, salinity increase with decreasing temperature cannot be solely explained by simple boiling. **Hedenquist and Henley** (**1985**) argued that boiling-induced salinity increases are relatively small compared to the larger salinity variations observed here (see **Figure 11**). With decreasing pressure and temperature during fluid ascent, the physical state of the hydrothermal solution undergoes substantial modification. Among the most critical of these changes is boiling, which leads to the separation of liquid and vapour phases. This process plays a key role in ore-forming systems, as it alters the chemical composition of the hydrothermal fluid and creates favourable conditions for metal precipitation. Primary boiling refers to the initial phase separation or vapour formation that occurs due to a reduction in hydrostatic or

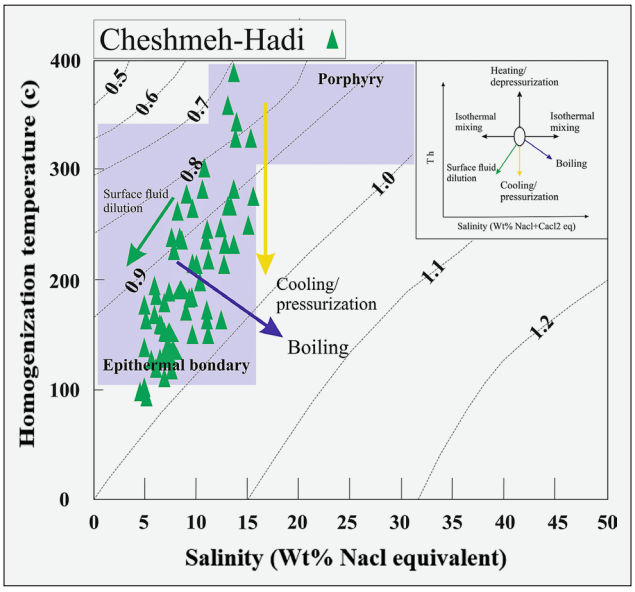

Figure 11. Homogenization temperature-salinity plot showing fluid densities (The fluid densities are shown with dashed lines) ranging from 0.7 to 1.0 g/cm³ in the Cheshmeh-Hadi copper deposit (**after Zhang and Frantz, 1987**), Homogenization temperature-salinity diagram (**Bodnar, 1983**) indicating boiling and cooling processes in the studied deposit, Homogenization temperature-salinity plot delineating the magmatic to epithermal fluid range in the deposit (**after Lattanzi, 1991**).

lithostatic pressure as the hydrothermal fluid ascends from deeper crustal levels. This phenomenon commonly takes place in systems characterized by steep thermal gradients, such as volcanic environments and hydrothermal vein systems. In contrast, secondary boiling develops when the hydrothermal fluid re-enters an unstable state as a consequence of fluid–rock interaction, structural discontinuities (e.g. fractures), or changes in temperature and fluid chemistry. Under these conditions, a new vapour phase may form without a significant large-scale pressure drop. This type of boiling is primarily driven by internal chemical reactions or fluid mixing

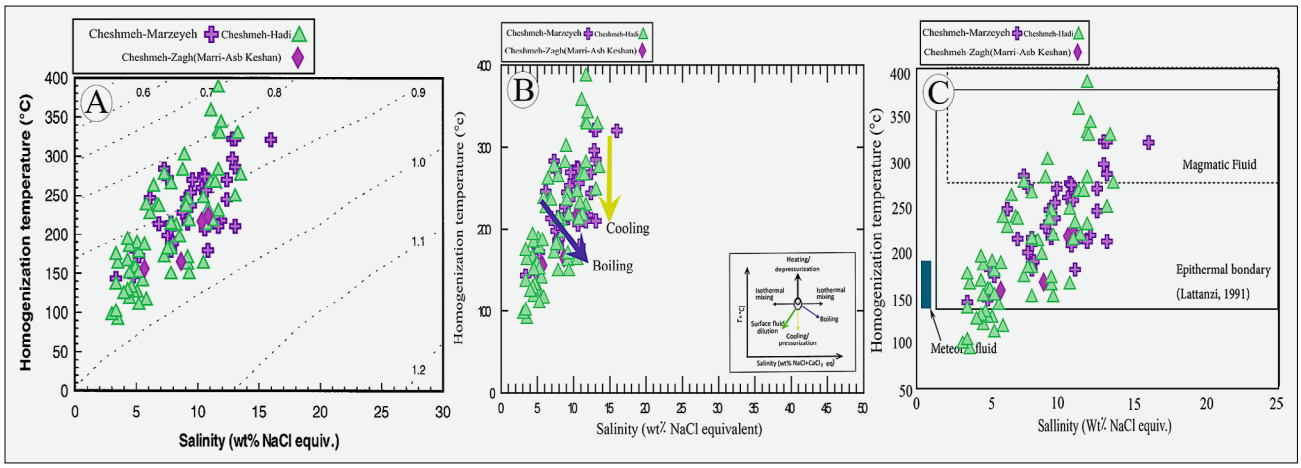

Figure 12. (**A**) Homogenization temperature versus salinity diagram for determining dominant metal complexes (after **Pirajno, 2009**). (**B**) Homogenization temperature versus salinity plot of various deposit types (**Wilkinson, 2001**), with the Cheshmeh-Hadi copper deposit samples falling within the epithermal deposit field. (**C**) Salinity versus homogenization temperature diagram of fluid inclusions showing different fluid-type fields (**after Beane, 1983**)

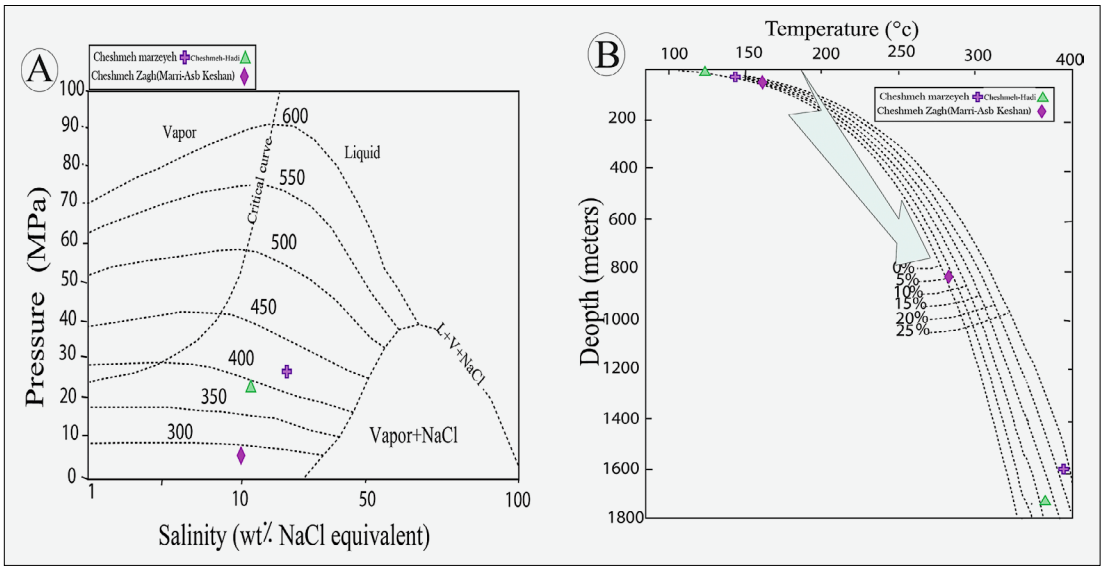

Figure 13. (**A**) Pressure versus salinity diagram showing fluid inclusion pressures of 26/5–28/5 MPa in the Cheshmeh-Hadi copper deposit (**after Zang and Frantz, 1987**). (**B**) Homogenization temperature versus depth diagram for estimating trapping depth of fluids in the Cheshmeh-Hadi copper deposit (**after Haas, 1971**)

processes. It typically occurs where hydrothermal fluids interact or mix with cooler or meteoric waters, or where water–rock reactions induce chemical disequilibrium and vapour generation.

The homogenization temperature–salinity diagram reflects a progressive cooling and dilution of the mineralizing fluid, with both temperature and salinity declining during late-stage deposition (see **Figure 11**). Hydrothermal systems dominated by hydrostatic pressure commonly experience boiling, and vapour pressure can be used to estimate trapping depths. Such systems generally relate to near-surface environments within the upper ~3 km of the crust (**Kant et al., 2012; Wilkinson, 2001**).

To identify the dominant metal-bearing complex, fluid inclusion data were plotted on **Pirajno's (2009)** diagram, showing that Cheshmeh-Hadi fluids fall within the sulfide complex field (see **Figure 12A**). According to **Wilkinson's (2001)** classification of ore-forming systems based on salinity and homogenization temperature, the Cheshmeh-Hadi samples fall within the epithermal deposit range (see **Figures 12B, C**). Origin determination using **Kesler's (2005)** diagram indicates that the fluids derive from magmatic waters, metamorphic waters, and meteoric waters, which likely reacted with host rocks during ascent, migrating along faults and fractures to deposit metals at the contact between conglomerate, andesite, agglomerate, and numulitic limestone.

The coexistence of liquid-rich, vapour-rich, two-phase inclusions with varying fill volumes, as well as some homogenized vapour inclusions, confirms boiling

Table 2. Sulfur isotopic composition ($\delta^{34}S$ ‰) of sulfide minerals in the Cheshmeh-Hadi copper deposit

Chalcopyrite<=>H_2S(**Li & Liu, 2006**)									
Sample Point	Mineral	$\delta^{34}S$min(‰)	T(°C)*-Min	T(°C)*-Ave	T(°C)*-Max	1000 Ln α-T(min)	1000 Ln α-T(Ave)	1000 Ln α-T(max)	$\delta^{34}SH_2S$fluid(‰)
CH-H-S17B	Chalcocite-Bornite-Chalcopyrite-Covellite-Silica(Quartz)	-23.8 ± 0.3	102	193.79	279	0.4	0.2	0.2	-24.0 ± 0.3
Galena<=>H_2S(**Li & Liu, 2006**)									
Sample Point	Mineral	$\delta^{34}S$min(‰)	T(°C)*-Min	T(°C)*-Ave	T(°C)*-Max	1000 Ln α-T(min)	1000 Ln α-T(Ave)	1000 Ln α-T(max)	$\delta^{34}SH_2S$fluid(‰)
CH-H-S17B	Chalcocite-Bornite-Chalcopyrite-Covellite-Silica(Quartz)	-23.8 ± 0.3	102	193.79	279	-4.6	-2.9	-2.1	-21.1 ± 0.3
Galena<=>Chalcopyrite(**Li & Liu, 2006**)									
Sample Point	Mineral	$\delta^{34}S$min(‰)	T(°C)*-Min	T(°C)*-Ave	T(°C)*-Max	1000 Ln α-T(min)	1000 Ln α-T(Ave)	1000 Ln α-T(max)	$\delta^{34}SH_2S$fluid(‰)
CH-H-S17B	Chalcocite-Bornite-Chalcopyrite-Covellite-Silica(Quartz)	-23.8 ± 0.3	102	193.79	279	-3.3	-1.5	-0.6	-22.3 ± 0.3

processes in the study area. Using the **Hass (1971)** diagram, the depth of mineralization in Cheshmeh-Hadi was estimated based on homogenization temperatures ranging from 90 to 386°C. The most frequent homogenization temperature range (100–300°C) corresponds to trapping depths between ~100 and 1580 meters (see **Figure 13A**). This suggests sulfate (SO_4^{2-}) or bisulfide (HS^-) as the dominant anions, consistent with the presence of minerals such as chalcocite and bornite. Using homogenization temperatures and boiling point data, and applying **Hass (1971)**, the trapping pressure of fluid inclusions was calculated via $P = H\rho g$, yielding pressures between 235 and 265 bar (see **Figure 13B**). The relationship between homogenization temperature and pressure is illustrated in **Figure 13**.

4.4. Stable Isotopes

4.4.1. Sulfur Isotopes

In order to investigate the origin and nature of ore-forming and alteration-related fluids in the Cheshmeh-Hadi copper deposit, sulfur and oxygen isotope analyses were performed. One sulfide mineral sample and two silica mineral samples were selected. Sample preparation was carried out at the laboratory in Tehran, and the specimens were subsequently sent to the Stable Isotope Research Laboratory at Arak University for isotopic analysis (see **Table 2**). Sulfur isotope fractionation occurs via two principal mechanisms that result in natural variations of $\delta^{34}S$ values in different environments and materials (**Hoefs, 2004**): (a) Abiotic isotopic fractionation, which takes place through various chemical exchange reactions between sulfate and sulfide species, or among different types of sulfides;

(b) Biological (kinetic) isotopic fractionation, which occurs through microbial metabolic processes, leading to the preferential incorporation of lighter sulfur isotopes (^{32}S) into biologically-derived products. In hydrothermal systems, sulfur is primarily present in reduced forms such as H_2S, HS^-, and S^{2-}, which play key roles in ore deposition processes (**Meheut et al., 2007**). The most stable sulfur species in reducing and alkaline environments are H_2S and HS^-. Under these conditions, the oxygen fugacity (fO_2) and pH of the hydrothermal fluids tend to be low, and the $\delta^{34}S$ values of deposited sulfide minerals generally reflect those of the total sulfur in the fluid (**Li and Liu, 2006**).

The sulfide minerals in the Cheshmeh-Hadi copper deposit exhibit a relative depletion in the heavy sulfur isotope (^{34}S). One of the plausible explanations for this isotopic depletion is the derivation of hydrothermal sulfur from the leaching of sulfide minerals in reduced sedimentary environments (**Hoefs, 2004**). The $\delta^{34}S$ values of H_2S in the ore-forming hydrothermal fluid are estimated to range from –22.6‰ to –2.7‰. In comparison, the $\delta^{34}S$ values in peridotitic kimberlites of mantle origin are approximately 0 ± 1‰, and in basaltic rocks typically vary between 0‰ and 5‰ (**Hoefs, 2004**). However, the recy-

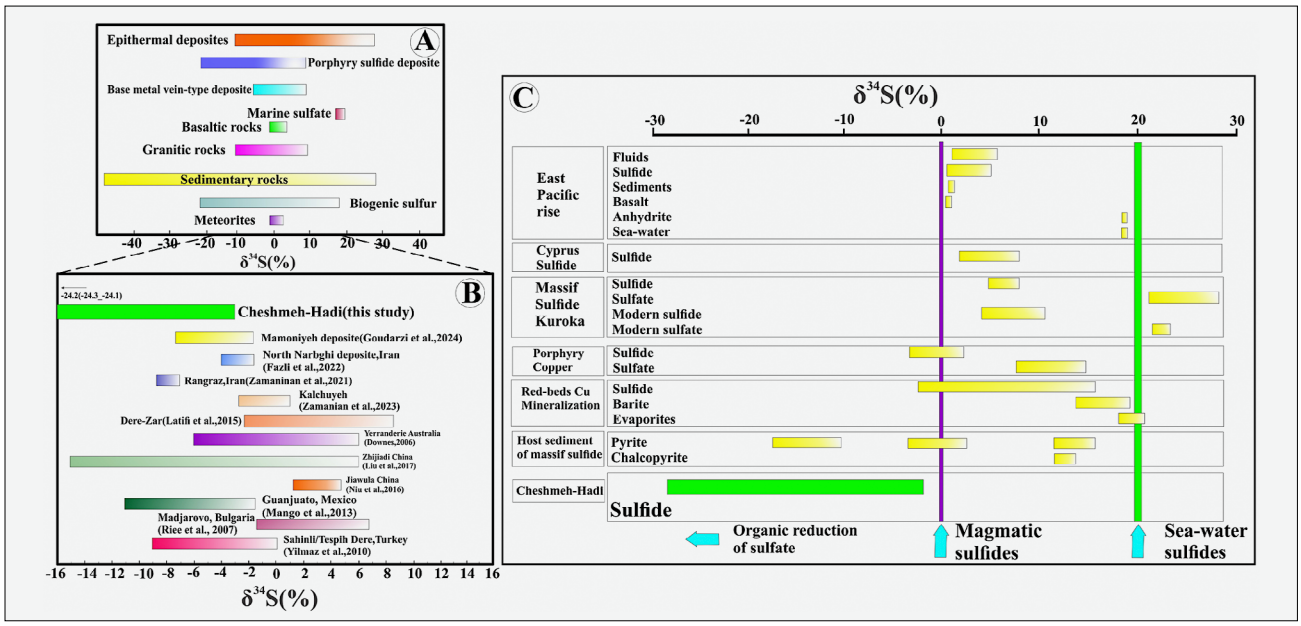

Figure 14. (**A**) Comparison of $\delta^{34}S$ values of sulfur in sulfides from various rock types (**Marini et al., 2011; Hoefs, 2021**). The data illustrate the typical sulfur isotope compositions for mantle-derived, magmatic, and crustal sources, showing distinct isotopic fields. (**B**) Sulfur isotopic compositions ($\delta^{34}S$) of sulfide minerals from the Cheshmeh-Hadi copper deposit compared to global epithermal deposits and deposits within the Urumieh-Dokhtar magmatic arc. The $\delta^{34}S$ values of Cheshmeh-Hadi sulfides fall within or near the compositional fields typical of hydrothermal systems, suggesting a similar fluid evolution pathway. (**C**) Comparison of $\delta^{34}S$ values of sulfides from the Cheshmeh-Hadi deposit with various geological environments (**Rollinson, 1993**). The data suggest that the sulfur isotopic signature of the Cheshmeh-Hadi sulfides is consistent with sources related to ilmenite-series granites and volcanic-hosted hydrothermal systems

cling of crustal materials (e.g. sulfides and marine sulfates) in subduction zones, as well as mantle contamination, can lead to significant heterogeneity in mantle sulfur isotopic values ranging from –10‰ to +10‰ (**Ohmoto and Goldhaber, 1997**). Therefore, the isotopic composition of the hydrothermal fluid may suggest a magmatic origin. Sulfur in the Cheshmeh-Hadi deposit may have been derived either from the leaching of primary volcanic-hosted sulfide minerals or directly from magmatic-hydrothermal fluids. One contributing factor to the ^{34}S depletion could be the preferential leaching of ^{32}S (due to its higher reactivity compared to ^{34}S; (**Hoefs, 2004**) from volcanic and pyroclastic host rocks by meteoric-dominated hydrothermal fluids. Another factor may be isotopic fractionation between sulfate and sulfide species in the hydrothermal fluid. Following isotopic equilibrium fractionation, and subsequent ^{34}S-depletion in sulfides, two potential scenarios could have occurred:

(a) During sulfide mineralization, the hydrothermal fluid expelled and dispersed the sulfate phase away from the vein system. The scarcity of sulfate minerals alongside sulfides may support this removal of sulfate-bearing fluids during or after mineralization. This scenario is consistent with acidic and oxidizing conditions facilitating sulfide precipitation from sulfur complexes and promoting sulfate phase separation.

(b) Prior to the current stage of sulfide deposition, the sulfate phase may have been precipitated at greater depths, allowing the upward migration of a sulfide-dominant hydrothermal fluid into the vein system, where it precipitated ^{34}S-depleted sulfide minerals.

Another mechanism possibly responsible for the observed ^{34}S depletion is the derivation of sulfur from sedimentary sequences containing biogenic sulfides, leached by meteoric-dominated hydrothermal fluids. However, given the fluid inclusion temperatures and the absence of sulfur-bearing sedimentary host rocks, a biogenic sulfur source and bacterial reduction processes are unlikely. Instead, the mixing of meteoric and magmatic waters likely produced a system in which both sulfate and reduced sulfur were generated. The $\delta^{34}S$ values of sulfide minerals in the Cheshmeh-Hadi deposit, when compared to various geological environments and sulfur sources, closely resemble those from ilmenite-series granites and hydrothermal sulfides (see **Figure 14A, B, C**). Additionally, **Figure 15** compares the $\delta^{34}S$ values of Cheshmeh-Hadi with those from other deposits in Central Iran, the Urumieh–Dokhtar belt, and other global analogues. These comparisons suggest that sulfide mineralization in the Cheshmeh-Hadi deposit was formed from fluids that derived sulfur predominantly via the reduction of seawater sulfate.

4.4.2. Oxygen Isotopes

The oxygen isotope compositions ($\delta^{18}O$) of hydrothermal fluids associated with altered and mineralized carbonate samples from the Cheshmeh Hadi copper deposit are presented in **Table 3**. The $\delta^{18}O$ values of mineralized samples fall within or close to the compositional fields of

meteoric water, basalts, and sedimentary rocks, suggesting that the hydrothermal fluids involved in ore deposition were primarily of magmatic origin but underwent mixing with meteoric waters. The $\delta^{18}O$ values of altered but barren carbonate samples plot entirely within the meteoric water range, slightly shifting toward magmatic compositions, indicating that carbonate alteration may have resulted from interaction between magmatic and meteoric fluids. This isotopic transition is consistent with the fluid inclusion microthermometry data, which indicate decreasing fluid temperatures due to fluid mixing and dilution. The evolution from a magmatic-dominated fluid to cooler, oxidizing, and more diluted meteoric waters is characteristic of hydrothermal systems where ore precipitation is triggered by fluid mixing, cooling, and changes in redox conditions (see **Figure 15**).

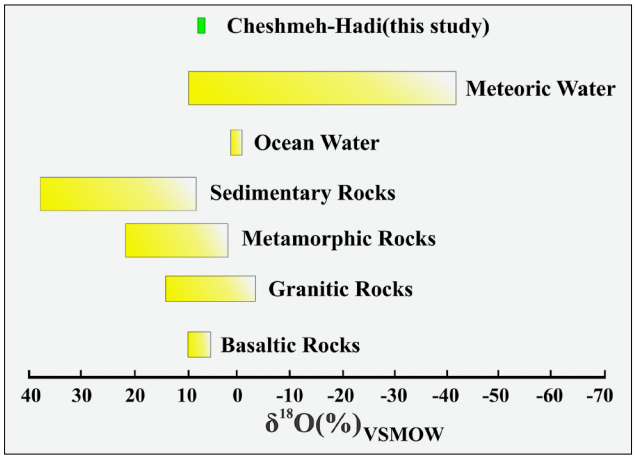

Figure 15. Comparison of $\delta^{18}O$ values from the Cheshmeh-Hadi copper deposit with various geological environments (**after Hoefs, 2004**)

The $\delta^{34}S$ values for three chalcopyrite samples from the main mineralization stage, after temperature correction, range narrowly between –24.3‰ and –2.6‰. These samples are located within evaporitic or sedimentary units containing sulfides of organic origin (**Oyarzun et al., 1998**). Oxygen isotope data from the Cheshmeh Hadi deposit indicate that the hydrothermal fluid responsible for mineralization had a meteoric origin. As it passed through sedimentary rocks, its heavy oxygen content increased (**Kojima et al., 2009**). The fluid became warmer as it moved downward, and the possible presence of cooling intrusive bodies at depth may also have contributed to fluid heating. During its downward circulation through sedimentary and volcanic units, the hydrothermal fluid leached copper from the host rocks and transported it. Isotopic data suggest that the sulfide necessary for mineralization was derived from the reduction of sulfate present in marine and evaporitic sediments; therefore, sulfate- and carbonate-bearing rocks played a key role in mineralization (carbonate-rich environments provided reducing conditions favourable for the conversion of sulfate to sulfide). Subsequently, as the hydrothermal fluid moved upward, copper-bearing minerals- mainly chalcopyrite and minor amounts of chalcocite- were deposited in fractures and cavities of the host rocks in primary or hypogene form. Upon exposure to near-surface conditions, these sulfide minerals were partially oxidized to secondary oxide minerals such as malachite, azurite, and covellite, forming a supergene enrichment zone.

4.5. Geochemistry of Major and Trace Elements

Eight samples from volcanic outcrops and drill cores were selected for petrographic and geochemical analyses of major and trace elements (see **Table 4**).

Table 3. Oxygen isotope compositions of hydrothermal fluids in equilibrium with host rocks in the Cheshmeh-Hadi copper deposit

Muscovite<=>H_2O(**Zheng, 1993b**)									
Sample Point	Mineral	$\delta^{18}O$min(‰)	T(°C)*-Min	T(°C)*-Ave	T(°C)*-Max	1000 Ln α-T(min)	1000 Ln α-T(Ave)	1000 Ln α-T(max)	$\delta^{18}OH_2O$fluid(‰)
CH.H-S13A	Silica(Quartz)	+7.6 ± 0.0	89	177.3	387	12.4	5.6	0.1	+2.0 ± 0.0
CH.H-S17A	Chalcocite-Bornite-Chalcopyrite-Covellite-Silica(Quartz)	+7.7 ± 0.3	102	193.69	279	11.3	4.8	1.9	+2.9 ± 0.3
Quartz<=>H_2O (**Meheut et al., 2007**)									
Sample Point	Mineral	$\delta^{18}O$min(‰)	T(°C)*-Min	T(°C)*-Ave	T(°C)*-Max	1000 Ln α-T(min)	1000 Ln α-T(Ave)	1000 Ln α-T(max)	$\delta^{18}OH_2O$fluid(‰)
CH.H-S13A	Silica(Quartz)	+7.6 ± 0.0	89	177.3	387	24.4	13.5	2.8	-6.2 ± 0.0
CH.H-S17A	Chalcocite-Bornite-Chalcopyrite-Covellite-Silica(Quartz)	+7.7 ± 0.3	102	193.69	279	22.9	12.1	6.5	-4.6 ± 0.3

Table 4. Chemical Analysis Results of the Studied Samples from the Cheshmeh-Hadi Copper Deposit (major elements in wt.%, trace ppm)

Sample	SiO_2	Al_2O_3	Na_2O	MgO	K_2O	TiO_2	CaO	Fe_2O_3	Ag	Pb	Cu	Mo	Bi	Fe	Co	Ni	Ti	Sb
CH.H-18	63.98	18.01	3.94	0.45	3.67	0.59	2.97	5.21	0.59	14.98	1069	2.21	0.06	35894	8.21	30	4466	1.11
CH.H-19	64.01	17.66	3.78	0.25	3.18	0.64	2.75	7.12	31.8	23.05	576	3.81	0.06	35758	4.21	19	3149	2.21
CH.H-21	57.94	16.83	3.47	0.02	4.13	0.75	2.35	5.45	0.18	37.98	1275	6.83	0.47	41600	4.91	13.89	3810	1.34
CH.H-26	61.43	17.21	5.47	1.45	3.68	0.64	5.74	4.27	0.41	21.95	545	3.03	0.18	38900	8.42	19.74	4010	0.57
CH.H-32	60.87	16.76	5.03	0.04	4.67	0.66	6.84	4.98	0.42	19.96	581	3.79	0.14	35700	6.23	16.27	3910	0.83
CH.H-33	60.11	18.18	5.19	1.65	3.78	0.67	6.03	4.75	0.44	22.1	465	3.28	0.15	31958	4.25	17.38	3410	0.85
CH.H-35	60.98	18.81	6.01	0.04	4.98	0.74	5.27	3.25	0.48	14.1	1067	2.14	0.06	3524	2.34	29.9	3225	1.48
CH.H-37	63.66	18.58	4.78	0.34	4.05	0.57	2.71	6.14	0.13	17.2	401	2.82	0.12	32354	9.91	18.84	0.49	1.82

Table 4. (continued)

Tl	Li	Be	Na	K	Ca	Mg	Al	Ga	Cs	Rb	Ba	Sr	Th	U	Y	Zr	Hf	Nb	Ta
0.54	11.02	4.92	31398	34735	24984	2869	7471	15.18	4.82	94.1	614	317	4.35	1.26	14.39	119.5	3.09	5.49	0.39
0.4	10.1	3.92	27589	28341	18036	1854	6503	15.19	3.92	79.2	421	316	4.29	1.55	14.49	18.5	3.13	4.59	0.3
0.59	15.87	1.12	32795	35286	13581	2397	2.67	15.17	5.41	74.4	255	133	2.7	0.35	8.69	109.6	3.79	4.68	0.45
0.5	22.69	1.43	36787	36297	47742	2386	4.18	18.58	5.69	78.3	369	224	3.9	0.34	17.99	128.5	3.67	5.39	0.42
0.57	18.54	1.24	35883	38176	34536	1396	2.59	17.28	6.71	101.3	401	185	3.2	0.26	14.98	110.6	3.16	4.88	0.36
0.55	17.35	1.51	35852	37609	35087	1288	2.38	16.18	6.8	122.2	362	191	3.2	0.24	14.99	110.5	3.16	5.29	0.24
0.38	10.1	3.91	30426	36678	23252	2779	7373	14.37	4.2	802.3	514	313	3.9	1.33	13.98	100.4	3.1	5.19	0.25
0.55	20.68	1.42	29138	42154	32243	4097	3459	17.76	5.61	86.4	399	174	4.5	0.24	20.59	142.35	4.17	5.97	0.47

Table 4. (continued)

P	La	Ce	Pr	Nd	Sm	Eu	Er	Gd	Tb	Dy	Ho	Tm	Yb	Lu
1095	12.05	29.9	3.92	13.71	2.97	0.97	1.67	3.27	0.48	3.05	3.38	0.28	1.81	0.3
1242	11.04	25.95	3.6	12.62	2.88	0.94	1.62	3.28	0.47	3.04	3.37	0.28	1.72	0.27
1006	4.64	9.88	1.3	5.82	1046	0.61	1.31	3.21	0.28	1.83	3.38	0.23	1.42	0.24
1010	8.93	19.48	2.55	11.01	3.01	1.01	2.35	3.1	0.52	3.36	3.67	0.34	2.31	0.37
802	5.61	13.49	1.84	8.03	2.34	0.94	1.78	3.22	0.43	2.76	0.56	0.31	1.83	0.32
904	6.12	12.48	1.72	9.27	2.34	0.76	1.81	3.12	0.34	2.43	0.57	0.23	2.05	0.24
1036	12.04	31.99	2.88	12.83	2.68	0.99	1.57	3.14	0.43	2.79	0.33	0.26	1.61	0.31
1014	7.44	17.96	2.29	10.86	2.23	1.01	2.63	3.37	0.51	3.28	0.73	0.34	2.6	0.42
1095	12.05	29.9	3.92	13.71	2.97	0.97	1.67	3.27	0.48	3.05	3.38	0.28	1.81	0.3
1242	11.04	25.95	3.6	12.62	2/88	0.94	1.62	3.28	0.47	3.04	3.37	0.28	1.72	0.27
1006	4.64	9.88	1.3	5.82	1046	0.61	1.31	3.21	0.28	1.83	3.38	0.23	1.42	0.24

For rock classification and minimizing alteration effects, immobile elements were used. Based on the Nb/Y vs. Zr/Ti diagram (**Pearce, 1996**), the volcanic rocks are classified mainly as andesite, basaltic andesite, basalt, and alkali basalt (see **Figure 16A**). Using the Nb/Y vs. Zr/TiO_2 plot (**Winchester and Floyd, 1977**), the samples are sub-alkaline basalt, basaltic andesite, and andesite (see **Figure 16B**). The Zr/TiO_2 vs. SiO_2 plot indicates compositions ranging from andesite to dacite and rhyodacite (see **Figure 16C**). Based on Co vs. Th (**Hasite et al., 2007**), the samples fall within the calc-alkaline basalt–andesite–andesite series (see **Figure 16D**).

To distinguish between continental arc and island arc settings, Ta/Yb vs. Th/Yb (see **Figure 16E**) and Zr vs. Zr/Y (see **Figure 16F**) diagrams (**Pearce, 1983**) were used. The samples plot in the continental arc field, indicating a source in enriched mantle influenced by subduction-zone fluids. High Th contents likely result from crustal contamination and subducted slab-derived fluids. Magmas from active continental margins typically show stronger enrichment in incompatible LREEs compared to island arc magmas, likely due to a combination of enriched mantle sources and crustal assimilation. The Zr vs. Zr/Y plot further confirms their placement within the continental volcanic arc field.

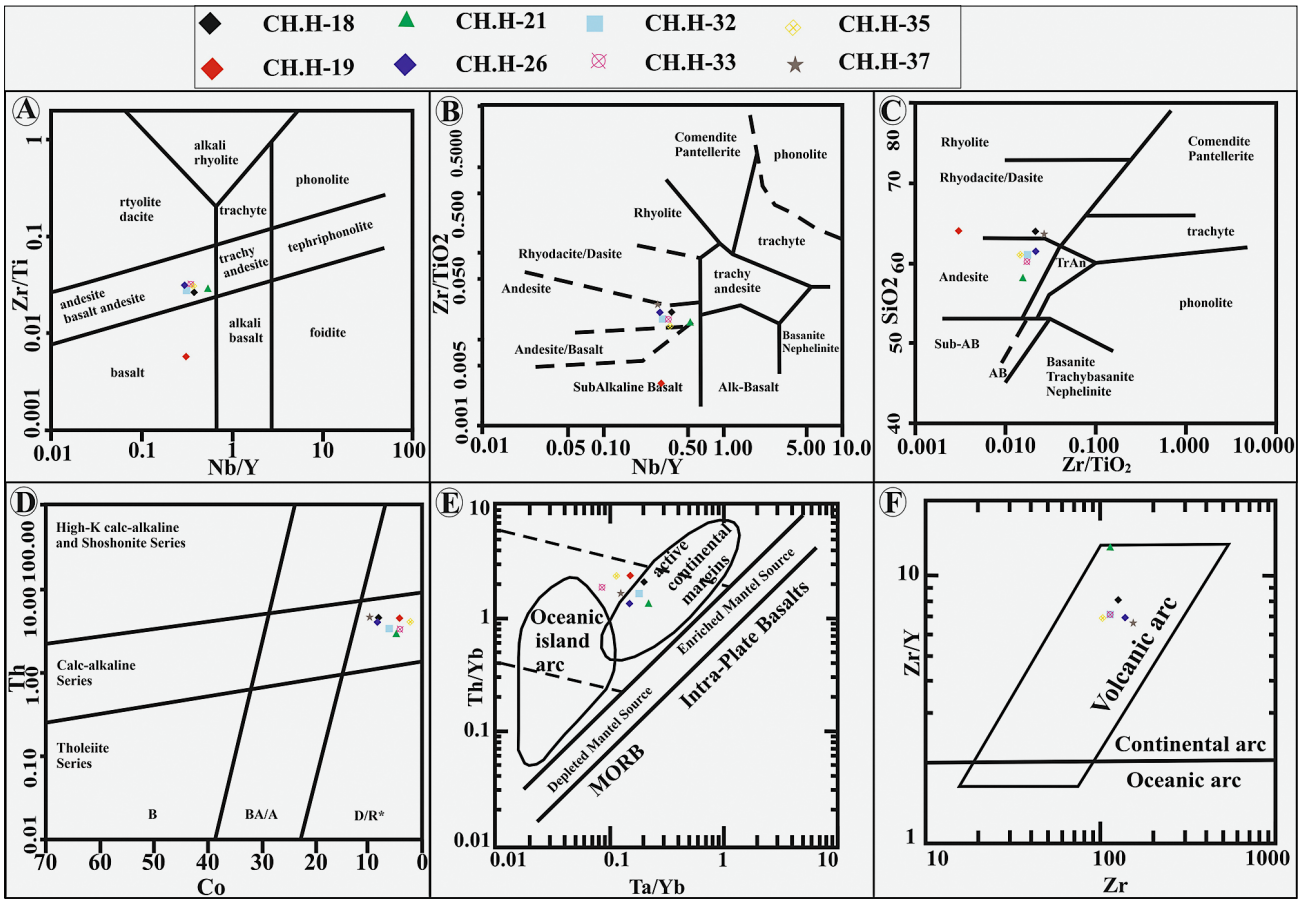

Figure 16. Geochemical discrimination diagrams used to identify the magma series and tectonomagmatic nature of the volcanic rocks in the Cheshmeh-Hadi copper deposit: (A) Nb/Y vs. Zr/Ti (**Pearce, 1996**), (B) Nb/Y vs. Zr/TiO_2 (**Winchester and Floyd, 1977**), (C) Zr/TiO_2 vs. SiO_2 (**Winchester and Floyd, 1977**), (D) Co vs. Th (**Hasite et al., 2007**), (E) Ta/Yb vs. Th/Yb (**Pearce, 1983**), (F) Zr vs. Zr/Y (**Pearce, 1983**)

The SiO_2 content in the volcanic rocks ranges from 57.94 to 64.01 wt%, with an average of 61.62 wt%. Al_2O_3 varies between 16.76 and 18.81 wt%, CaO from 2.35 to 6.84 wt%, Na_2O from 3.47 to 6.01 wt%, K_2O from 3.18 to 4.98 wt%, MgO from 0.02 to 1.65 wt%, TiO_2 from 0.57 to 0.75 wt%, and total Fe_2O_3 (Fe_2O_3T) from 3.25 to 7.12 wt%. To understand the processes influencing magma evolution, such as fractional crystallization, binary plots of oxide- oxide, oxide- element, and element- element Harker diagrams (**Harker, 1909**) were utilized. Generally, linear or negatively correlated trends suggest the influence of processes like fractional crystallization, magma mixing, or crustal assimilation. However, significant scattering may reflect crystal accumulation, alteration, or crustal contamination (**Willson, 2007**). Among the major oxides, Na_2O and Al_2O_3 show increasing trends (see **Figure 17C, E**). K_2O versus SiO_2 lacks a clear trend and shows scattered values (see **Figure 17F**). In calc-alkaline suites, the concentrations of MgO, CaO, Fe_2O_3, and TiO_2 decrease with increasing SiO_2, which aligns with the volcanic rocks of the Cheshmeh-Hadi deposit (**Feely et al., 2002**), reflecting the crystallization of ferromagnesian minerals and plagioclase, amphibole, and clinopyroxene fractionation (see **Figure 17A, B**). The decreasing CaO trend corresponds to plagioclase crystallization from anorthite to albite (see **Figure 17D**). The increasing trends in Na_2O and possibly K_2O may be attributed to the presence of alkali feldspar in the final stages of crystallization or potassium addition during hydrothermal alteration (**Feely et al., 2002**). These trends overall highlight the role of continental crust in the magmatic evolution. In the SiO_2 vs. Sr diagram (see **Figure 17G**), Sr shows a decreasing trend consistent with plagioclase fractionation at low pressure. Since Sr is compatible in plagioclase but not in clinopyroxene, this trend also matches the decreasing CaO pattern due to plagioclase evolution. Europium (Eu) first increases with increasing SiO_2 and then decreases, reflecting plagioclase involvement in magma evolution, further supported by a positive correlation between Sr and Eu (see **Figure 17H**). The Dy/Yb ratio shows a slight decrease with increasing SiO_2, indicating hornblende or clinopyroxene fractionation (see **Figure 17I**). The Sr content also decreases with MgO, suggesting plagioclase removal (see **Figure 17J**). The Rb/Sr ratio first decreases and then increases with increasing Sr, displaying an almost linear trend consistent with plagioclase, hornblende, and clinopyroxene fractionation (**Davidson**

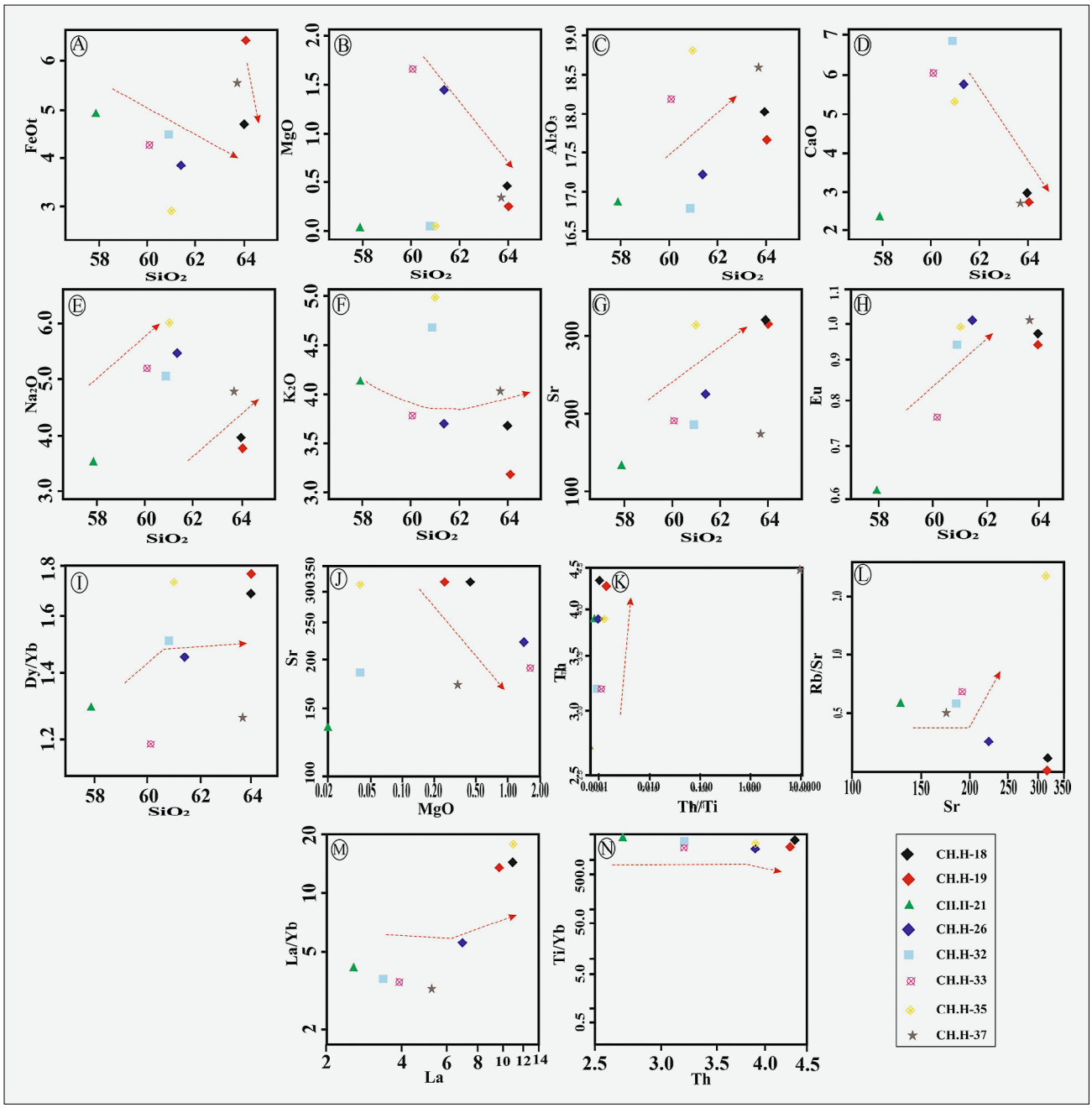

Figure 17. Harker variation diagrams used for petrogenetic interpretation of the volcanic rocks from the Cheshmeh-Hadi copper deposit: (A) SiO_2 vs. FeOt, (B) SiO_2 vs. MgO, (C) SiO_2 vs. Al_2O_3, (D) SiO_2 vs. CaO, (E) SiO_2 vs. Na_2O, (F) SiO_2 vs. K_2O, (G) SiO_2 vs. Sr, (H) SiO_2 vs. Eu, (I) SiO_2 vs. Dy/Yb, (J) MgO vs. Sr, (K) Th/Ti vs. Th, (L) Sr vs. Rb/Sr, (M) La vs. La/Yb, (N) Th vs. Ti/Yb. (**Stepanov et al., 2014; Klimm et al., 2008; Davidson et al., 2007; Wilson, 2007**)

et al., 2007) (see **Figure 17L**). The Th/Ti vs. Th (see **Figure 17K**), La vs. La/Yb (see **Figure 17M**), and Th vs. Ti/Yb (see **Figure 17N**) diagrams (**Schiano et al., 2010**) indicate crustal contamination during magmatic differentiation in the Cheshmeh-Hadi region. Spider diagrams normalized to primitive mantle (**Sun and McDonough, 1989**) show negative slopes with enrichment of LILEs over HFSEs, and depletion in HREEs, all features characteristic of calc-alkaline magmas. The observed positive Pb anomaly is indicative of crustal contamination during magma evolution (see **Figure 18A**). In the chondrite-normalized REE diagram, the volcanic rocks from Cheshmeh-Hadi exhibit moderate LREE enrichment, HREE depletion, and weak negative Eu anomalies, further reflecting plagioclase fractionation and a continental arc signature (see **Figure 18B**).

4.6. Tectono-Magmatic Model

Most of the known Manto-type copper deposits in Iran formed during the Eocene period – a time characterized by intense tectonic and magmatic activity, especially within the Urumieh-Dokhtar Magmatic Arc (UDMA),

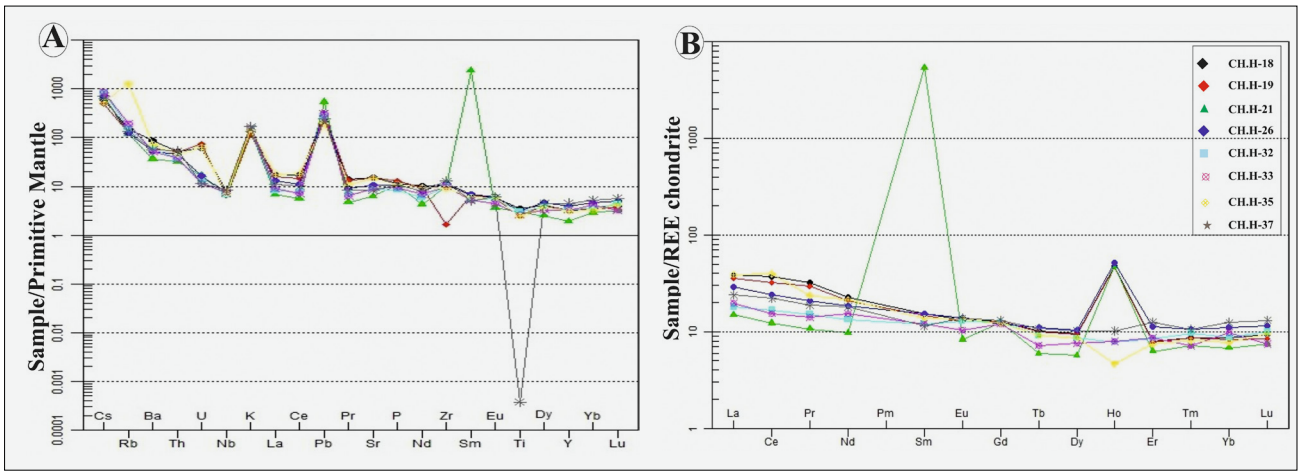

Figure 18. (**A**) Primitive mantle–normalized trace element patterns for rock samples from the Cheshmeh-Hadi deposit. Normalization values are from **Sun and McDonough (1989)**. (**B**) Chondrite-normalized rare earth element (REE) patterns for samples from the Cheshmeh-Hadi deposit, with chondrite values from **Boynton (1984)**

Alborz Magmatic Arc (AMA), and the Sabzevar region. The Eocene is considered a key metallogenic epoch due to the closure of the Neo-Tethys Ocean. Many of Iran's mineral deposits, including Manto-type copper deposits, are closely related to the evolution of the Neo-Tethys Ocean. These deposits typically form in arc-related or subduction zone settings and are generally associated with volcano-sedimentary environments along plate boundaries. They are often hosted by basaltic to andesitic rocks. The general formation process of Manto-type copper deposits involves the generation of calc-alkaline magma in the subduction zone, heat-induced alteration due to intrusive bodies, and the precipitation of copper along fractures and rock porosity through hydrothermal fluids derived from the mantle and lower crust. The Khaf–Doruneh Belt (in the southern Sabzevar Zone, northwest of Bardeskan) hosts Manto-type copper mineralization due to its tectonically active setting related to the subduction of Neo-Tethyan oceanic crust beneath the Central Iranian continental crust and the concurrent Eocene magmatic activity (see **Figure 19A**). These deposits are typically stratabound and hosted in volcanic and sedimentary sequences. The Sabzevar Ocean, situated between the Lut Block to the south and the Turan Block to the north, remained open since at least the mid-Cretaceous. Intra-oceanic subduction in the Sabzevar Basin likely began before the Albian, as evidenced by the presence of high-pressure metamorphic rocks (**Rossetti et al., 2010**). Similar to UDMA magmatism, the Eocene–Oligocene magmatic rocks in the Kashmar region of the Sabzevar area formed during Eocene extensional tectonics (**Shafaii Moghadam et al., 2015**). The Eocene volcanic activity in Davarzan–Abbasabad (Sabzevar) began with continental to shallow marine Paleogene–Eocene sediments and was followed by widespread subaqueous to subaerial basaltic and andesitic volcanism, volcaniclastic rocks, and sedimentary sequences during the middle to late Eocene (**Ghasemi and Rezaei-Kahkhaei, 2015**). These E–W-trending magmatic rocks were generated in response to the subduction of Neo-Tethyan oceanic lithosphere beneath the eastern Alborz (see **Figure 20B**). The mid-Eocene volcanic rocks of the Davarzan–Abbasabad area formed in a back-arc extensional setting and are associated with post-Eocene subduction-related magmatism (see **Figure 19B**). This region experienced collisional and post-collisional tectonic events during the Oligocene to Miocene (**Berberian and King, 1981; Ghasemi and Talbot, 2006; Asiabanha et al., 2012; Asiabanha and Foden, 2012; Ghasemi and Rezaei-Kahkhaei, 2015**). In western Sabzevar (Davarzan–Abbasabad area), these Eocene volcanic rocks host Manto-type Cu–Ag mineralization, including the Bozorg Mine, Damanjala, Asiadeyu, Labkalu, North Choghandarsar, South Choghandarsar, Elhak, and Dochileh deposits. Three main hypotheses have been proposed for the formation of Manto-type deposits: Syn-volcanic or syngenetic formation concurrent with volcanic activity (**Sato, 1984; Ruiz et al., 1971; Tosdal and Munizaga, 2003**). Formation through the action of intrusive bodies and their derived hydrothermal fluids (**Palacios, 1986, 1990; Oliveros et al., 2008**). Formation via leaching of copper from volcanic units during diagenetic processes (**Sato, 1984; Wilson and Zentilli, 2006; Wilson et al., 2003a, b; Kirkham, 1996; Tosdal and Munizaga, 2003**). The formation of the Cheshmeh Hadi deposit can be divided into two main stages: Hypogene stage – associated with volcanic activity, early diagenesis, and diagenetic alteration and Supergene stage – related to uplift and the influence of meteoric fluids.

4.6.1. Early Diagenesis

During the Eocene, a rift-related extensional environment developed behind the Sabzevar magmatic arc. As a result of volcanic activity, volcanic and pyroclastic rocks were deposited over the basement of this rifted setting.

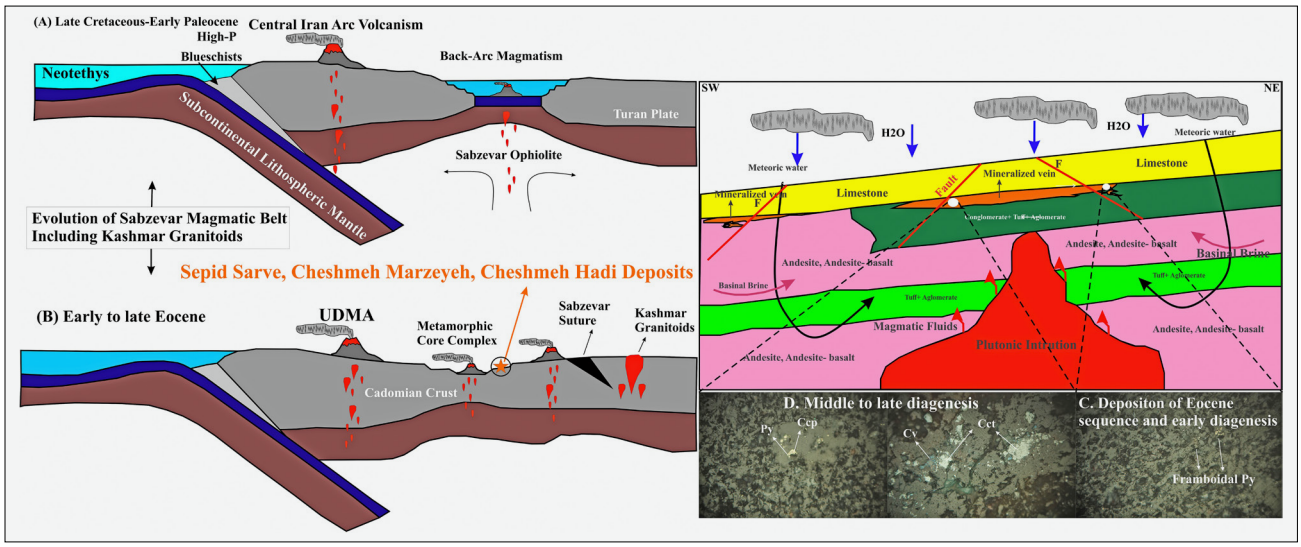

Figure 19. Schematic model illustrating the formation and evolution of the Sabzevar region: (**A**) Oblique subduction of the Neo-Tethyan lithosphere beneath the Iranian plate from Middle–Late Jurassic to Late Cretaceous, followed by the development of back-arc sedimentary and magmatic basins in the Sabzevar area. (**B**) From early to late Eocene, the Kashmar granites and associated volcanic rocks formed above a north-dipping subduction zone during a phase of magmatic flare-up triggered by regional extension (**Shafaii Moghadam et al., 2015**). These Eocene volcanic rocks host Manto-type Cu deposits in the Sepidsarv, Cheshmeh Marzih, and Cheshmeh Hadi areas. (**C-D**) The formation of the Cheshmeh Hadi deposit can be divided into two main stages: Hypogene stage – associated with volcanic activity, early diagenesis, and diagenetic alteration. Supergene stage – related to uplift and the influence of meteoric fluids.

These rocks contain minor amounts of copper, with Cu adsorbed at the surface of their silicate mineral networks. During this stage, along with the formation of the host rocks and early diagenesis, framboidal pyrites formed sporadically within the andesitic-tuffaceous matrix. In many mantle-type copper deposits, the sulfur necessary for pyrite formation is supplied by bacterial reduction of seawater sulfate, which reacts with available iron in the basin, ultimately producing pyrite in the host rock matrix (**Zentilli et al., 2009; Wilson et al., 2003a,b; Wilson and Zentilli, 1999; Corrillo-Rosua et al., 2014**). Since the Cheshmeh Hadi deposit formed in a shallow marine environment, this mechanism is likely applicable here as well. In this setting, pyrite formation plays a key role in establishing reducing conditions in the mineralized host rock. Following volcanic activity, limestone and shale sediments began to accumulate immediately in the subaqueous environment (see **Figure 19C**).

4.6.2. Intermediate and Late Diagenesis

In rift-related extensional environments, extensive volcanic activity leads to the formation of a thick volcanic-sedimentary sequence, which retains high amounts of heat (**Kirkham, 1996**). During this stage, pressure from diagenesis and dehydration of the underlying pyroclastic units generates hydrothermal fluids. The presence of zeolites in the host rock units indicates the progression of burial diagenesis. The mechanical breakdown of pyroclastic units in oxidizing coastal environments leads to silicate dissolution, forming clay minerals. During this reaction, Cu and Fe hydroxides are released, and Cu is adsorbed on clay minerals and Fe hydroxides. Due to the high ambient temperature and circulation through the volcanic sequence- especially the red layers- these fluids become enriched in copper, leaching it from the units and transporting it upward. Upon reaching porous and reducing andesitic-tuff units (where pyrite is present), the copper-bearing fluids precipitate Cu as sulfide. The oxidizing Cu-bearing fluid reacts with unstable pyrite, and sulfur from the pyrite reduces the fluid, resulting in copper sulfides replacing pyrite. Part of the pyrite's iron enters the sulfide network, and the remainder forms hematite (**Zentilli et al., 2009; Corrillo-Rosua, 2014**). The high concentration of hematite around Cu sulfides in the host rock supports this mechanism. Some copper also precipitates due to cooling of the hydrothermal fluid, as high-temperature hydrothermal fluids interact with trapped seawater in the host rock. This cooling destabilizes the chloride complexes transporting copper, leading to Cu sulfide precipitation. During this stage, copper sulfides form as disseminated grains, cavity-filling, and thin veins or veinlets within the host rock. The formation of these small veins is facilitated by the high burial pressure in the host rock during diagenetic mineralization (see **Figure 19D**).

4.6.3. Supergene Stage

This stage involves the uplift of the host rock units, tectonic processes, and weathering. With the onset of uplift, the andesitic host rock of the ore deposit becomes fractured along faults, creating abundant open spaces. During this stage, meteoric fluids leach copper from the

andesite-Conglomerate-Aglomerate host units and concentrate it in fractures and fault-related cracks. The veins formed at this stage typically have greater thickness due to the low confining pressure and are restricted to the mineralized host units. Additionally, primary sulfide minerals are altered into secondary sulfides such as digenite, covellite, malachite, as well as oxidized copper minerals (see **Figure 19D**).

5. Conclusion

The Cheshmeh-Hadi copper deposit is a strata-bound (Manto-type) sulfide system hosted in volcanic-sedimentary sequences formed in a subduction-related magmatic arc setting. The volcanic succession, predominantly comprising basalt, basaltic andesite, and andesite, developed in a non-marine environment, followed by deposition of sedimentary conglomerates and limestone. Mineralization is mainly associated with chlorite, zeolite, and calcite alteration zones. Copper mineralization occurs predominantly as fine-grained chalcocite within permeable conglomerates and, to a lesser extent, in limestones. The ore-forming fluids, characterized by low silica content and reducing conditions, ascended along faults, depositing copper in fractures and pore spaces. Geochemical and isotopic data suggest that the mineralizing fluids originated primarily from a magmatic source but underwent mixing with meteoric waters, promoting sulfide precipitation. Fluid inclusions indicate moderate salinities (3.09–13.39 wt.% NaCl eq.) and highlight boiling and fluid mixing as key mineralization mechanisms. Sulfur isotope values ($\delta^{34}S$ between –2.6‰ and –24.1‰) and oxygen isotope signatures support a model of magmatic-meteoric fluid interaction. Geochemical analyses confirm a calc-alkaline to shoshonitic affinity of volcanic rocks derived from an enriched mantle source influenced by subduction-related fluids and crustal contamination. Mineralogy is dominated by primary chalcocite, bornite, and pyrite, with supergene malachite, azurite, and hematite. Alteration includes regional zeolite–carbonate and localized chlorite and hematite zones. The Cheshmeh-Hadi deposit exemplifies copper mineralization in an active continental margin, where subduction-related magmatism, structural controls (notably the Doruneh Fault), and hydrothermal processes converge to form significant Manto-type deposits in volcano-sedimentary environments.

6. References

Abolipour, M., Rastad, E., Rashidnejad Omran, N. (2015). Manto-type copper mineralization in pyrobitumen-bearing porphyritic andesite, Koshkoiye district of Rafsanjan, Dehaj-Sardoiye subzone. *sciences. Q. J. Geosciences*. 24 (95), 123–144.

Aghanabati, A. (2004). Geology of Iran. *Geological Survey of Iran, Tehran, Iran*, 586 p.

Alavi, M. (1991). Sedimentary and structural characteristics of the Paleo Tethys remnants in northeastern Iran. *Geological Society of America Bulletin*, 103:983-992, https://doi.org/10.1130/0016-7606(1991)103<0983:SASCOT>2.3.CO;2.

Alizadeh, V., Momenzadeh, M., Emami, M.H. (2013). Petrography, geochemistry, mineralogy, fluid inclusions and mineralization study of Vorezg-Qayen copper deposit. *Sciences – Quarterly Journal of Geosciences*. 22 (86), 47–58.

Beane, R.E. (1983). The magmatic-meteoric transition. Geothermal Resources Council, *Special Report* 13, 245–253.

Bodnar, R.J. (1983). A method of calculating fluid inclusion volumes based on vapor bubble diameters and P-V-T-X properties on inclusion fluids. *Economic Geology* 78, 534–542, https://doi.org/10.2113/gsecongeo.78.3.535.

Boveiri Konari, M., Rastad, E., Rashidnejad Omran, N. (2011). Volcanic redbed-type copper mineralization in the Keshtmahaki, Southern Sanandaj-Sirjan Zone, southeastern Iran. *11 th SGA Biennial Meeting Let's Talk Ore Deposits.* 26-29 Sept, Antofagasta, Chile.

Boynton, W.V. (1984). Cosmochemistry of the rare earth elements, Meteorite studies. In: Henderson, P. (Ed.), Rare Earth Element Geochemistry. *Developments in Geochemistry. Elsevier, Amsterdam*, pp. 115–1522, https://doi.org/10.1016/B978-0-444-42148-7.50008-3.

Carrillo-Rosua, F.J. Morales-Ruano, S., Morata Cespedes, D., Boyce, A. J., Belmar, M., Fallick, A. E., Fenoll Hach-Ali, P., Munizaga, F., (2006). Sulfur isotope studies in Chilean "Manto"-type Cu–(Ag) deposits in coastal range of central Chile (area de la serena y Melipilla), *vol. 2, Actas XI Congreso Geologico Chileno, Antofagasta*, 199- 202.

Davidson, J., Turner, S., Handley, H., Macpherson, C. and Dosseto, A. (2007). Amphibole "sponge" *in arc crust Geology* 35: 787–790, https://doi.org/10.1130/G23637A.1.

Dissanayake, C.B. (1993). Gold and other metals in graphite. In: Parnell, J., Kucha, H. and Landais, P. (eds.), Bitumen in Ore Deposits. *Society for Geology Applied to Mineral Deposits*, SP. 9, 138–152, https://doi.org/10.1007/978-3-642-85806-2_9.

Downes, P. M., Yerranderie. (2007). a Late Devonian silver–gold–lead intermediate sulfidation epithermal district, eastern Lachlan Orogen, New South Wales, *Australia. Resource Geology*. 57(1), 1–23, https://doi.org/10.1111/j.1751-3928.2006.00001.x

Ebrahimi. S., Arab-Amiri. A., Ghanbari. H. (2020). Mineralogy, alteration, fluid inclusion and stable isotopes studies of the Sharifabad-Bardeskan copper deposit, NE Iran., *Scientific Quarterly Journal, GEOSCIENCES*. Vol. 30, No. 117, p:135-146.

Entezari Harsini, A. (2017). Geology, Geochemistry, Mineralization, Genesis and Isotope studies of Golcheshmeh deposit, South Neyshabour, Northeastern Iran. *Unpublished Ph.D. thesis, Ferdowsi University of Mashhad, Iran*. 310 p. (in Persian with English abstract).

Fazeli, A. (2002). Type of the copper mineralization at Veshnaveh deposit, south of Qom. [Unpublished M.Sc. thesis], *Tehran, Kharazmi university, Iran*. p. 157.

Fazli, N., Ghaderi, M., Movahednia, M., Maghfouri, S. (2021). Manto-type copper mineralization in the central part of the Urumieh-Dokhtar magmatic arc (Qom-Saveh region) with

emphasis on the East Narbaghi deposit, northeast Saveh. *Iranian Journal of Geology*. 15 (59), 69–90, https://doi.org/10.22059/ijg.302909.1072.

Fazli, N., Ghaderi, M., Movahednia, M., Li, J.W., Lentz, D.R., Yan, S. (2022). Geology and genesis of the North Narbaghi Cu-Ag deposit in the Urumieh-Dokhtar magmatic arc, Iran: fluid inclusion and stable isotope constraints. *Ore Geology Reviews.* 144, 104801, https://doi.org/10.1016/j.oregeorev.2022.104801.

Feely, T. C; Cosca, M. A. and Lindsay, C. R. (2002). Petrogenesis and implications of calc-alkaline cryptic hybrid magmas from Washburn volcano, Absaroka volcanic province, *U.S.A. Journal of Petrology*, 43(4), https://doi.org/10.1093/petrology/43.4.663.

Jabari, A., Malekzadeh Shafaroudi, A., & Karimpoor, M. H. (2016). The stratabound (mantle-type) copper deposit of Kal Abri in the Eocene volcano-sedimentary complex, NW Bardaskan, NE Iran. *Journal of Advanced Applied Geology*. 23.

Jiba, Z., Ghaderi, M., Maghfouri, S. (2021). Geology, mineralogy, and fluid inclusion studies of the Yamaghan Manto-type Cu (Ag) deposit, southeast Zanjan, NW Iran. *Advanced Applied Geology*. 11 (3), 594–615.

Haas, J.L. (1971). The effect of salinity on the maximum thermal gradient of a hydrothermal system at hydrostatic pressure. *Economic Geology* 66, 940-946, https://doi.org/10.2113/gsecongeo.66.6.940.

Harker, A. (1909). The Natural History of Igneous Rocks. *Macmillam*, https://doi.org/10.2307/1777000.

Hasite, A.R., Kerr, A.C., Pearce, J.A. and Mitchell, S.F. (2007). Classification of altered volcanic island arc rocks using immobile trace elements: development of the Th-Co discrimination diagram, *Journal of Petrology*, v. 48, p. 2341-2357, https://doi.org/10.1093/petrology/egm062.

Hedenquist J.W. and Henley R.W. (1985). The important of CO2 on freezing point measurements of fluid inclusion: evidence from active geothermal system and implication for epithermal ore deposition. *Economic Geology*., 80: 1379-1406, https://doi.org/10.2113/gsecongeo.80.5.1379.

Heidari, M. (2012). Study of Geochemistry, Sulfur Stable isotopes, and Genesis of Madan Bozorg Copper Deposit (Abbasabad, East of Shahroud). *Unpublished M.Sc. thesis, Bu-Ali Sina University, Iran*. 169 p. (in Persian with English abstract).

Herazo, A., Reich, M., Barra, F., Morata, D., Real, I.D., Pag` es, A. (2020). Assessing the role of bitumen in the formation of stratabound Cu-(Ag) deposits: Insights from the Lorena deposit, Las Luces district, northern Chile. *Ore Geology Reviews*. 124, 103639, https://doi.org/10.1016/j.oregeorev.2020.103639.

Hoefs, J. (2004). Stable Isotope Geochemistry, *Springer- Verlog, Berlin*, 287p, https://doi.org/10.1007/978-3-662-05406-2.

Hoefs, J. (2021). Stable Isotope Geochemistry (8th ed.). *Cham, Switzerland: Springer,* https://doi.org/10.1007/978-3-030-77692-3.

Ghasemi, H., Rezaei-Kahkhaei, M. (2015). Petrochemistry and tectonic setting of the Davarzan-Abbasabad Eocene Volcanic (DAEV) rocks, NE Iran. *Miner. Petrol*. 109, 235–252, https://doi.org/10.1007/s00710-014-0353-3.

Goudarzi M, Zamanian H, Kloetzli U, Lentz D. (2024). Eocene Magmatism and Ore forming Processes of copper at Mamuniyeh Area (Central Iran): *Using Trace Element and Isotopic Geochemistry of Zircon*, P.366, https://doi.org/10.1016/j.oregeorev.2024.106279.

Kaboodi, Z., Ghaderi, M., Rastad, E. (2019). Mineralogy, texture and structure and genetic model of Kahak Manto-type copper deposit in the Eocene volcano-sedimentary sequence, south Qom. *Geosciences – Scientific Quarterly Journal*. 29 (113), 145–154.

Kant, W., Warmada, W., Idrus, A., Setijadji, L.D., Watanabe, K. (2012). Fluid inclusion study of the polymetalic epithermal quartz veins at Soripesa Prospect Area, Sumbawa island, Indonesia. *Journal of Applied Geology* 4, 77-89, https://doi.org/10.22146/jag.7199.

Kesler S. E. (2005). Ore-forming fluids. Elements. 1(1), pp. 13-18, https://doi.org/10.2113/gselements.1.1.13.

Kirkham, R. V. (1996). Volcanic Red Bed copper. In: Geology of Canadian Mineral Deposit Types, (ed.) Eckstrand, O. R., Sinclair, W. D. and Thorpe, R. I.. *Geological Survey of Canada*, No. 8: 241- 252.

Klimm, K., Holtz, F., King, P.L. (2008). Fractionation vs. magma mixing in the Wangrah suite A-type granites, Lachlan Fold Belt. *Australia: experimental constraints. Lithos* 102, 415–434, https://doi.org/10.1016/j.lithos.2007.07.018.

Kojima, S., Tristá-Aguilera, D. and Hayashi, K. I. (2009). Genetic aspects of Manto type copper deposits based on geochemical studies of north Chilean deposits. Resource Geology 59: 87- 98, https://doi.org/10.1111/j.1751-3928.2008.00081.x.

Latifi Saii, F., Mirnejad, H., Alipour Asl, M., & Niroomand, S. (2014-2015). Evaluating the Au mineralization in the Darrehzar vein system (Pariz area – Kerman Province), with emphasis on fluid inclusion and sulfur isotope studies. *Advanced Applied Geology*, 4(4), 65–75.

Lattanzi, P. (1991). Applications of fluid inclusions in the study and exploration of mineral deposits. *Europian Journal of Mineral* 3, 689–697, https://doi.org/10.1127/ejm/3/4/0689.

Liu, Y., Zhang, J., & Li, Y. (2017). Genesis of the Zhijiadi Ag–Pb–Zn Deposit, Central North China Craton: Constraints from Fluid Inclusions and Stable Isotope Data. *Geofluids. Article ID 4153618,* https://doi.org/10.1155/2017/4153618.

Li YB, Liu JM. (2006). Calculation of sulfur isotope fractionation in sulfides. *Geochimica et Cosmochimica Acta* 70: 1789 – 1795, https://doi.org/10.1016/j.gca.2005.12.015.

Maghfouri, S., Movahednia, M. (2015). Investigation of geology and mineralization of Abbas Abad copper deposit and comparison with manto-type deposit. *18 th Symposium of the Geological Society of Iran, Tarbiat Modares University, Tehran, Iran* (in Persian with English abstract).

Maghfouri, S., Hosseinzadeh, M.R., Moayyed, M., Movahednia, M., Choulet, F. (2017). Geology, mineralization and sulfur isotopes geochemistry of the Mari Cu (Ag) Manto-type deposit, northern Zanjan, Iran. *Ore Geology Reviews*. 81, 10–22, https://doi.org/10.1016/j.oregeorev.2016.12.007.

Mango, H., Oreskes, N., & Zantop, H. (2013). Origin of epithermal Ag–Au–Cu–Pb–Zn mineralization in Guanajuato, Mexico. *Mineralium Deposita.* 49(1), 119–143, https://doi.org/10.1007/s00126-013-0502-2.

Marini, L., Moretti, R., Accornero, M. (2011). Sulfur isotopes in magmatic-hydrothermal systems, melts, and magmas. *Rev. Mineral. Geochem*. 73, 423–492. https://doi:10.1515/9781501508370-014.

Méheut M, Lazzeri M, Balan E, Mauri F. (2007). Equilibrium isotopic fractionation in the kaolinite, quartz, water system: Prediction from first-principles density-functional theory. *Geochimica et Cosmochimica Acta* 71: 3170-3181, https://doi.org/10.1016/j.gca.2007.04.012.

Merinero, R., Ortega, L., Lunar, R., Pi˜na, R., C´ardenes, V. (2019). Framboidal chalcopyrite and bornite constrain redox conditions during formation of their host rocks in the copper stratabound mineralization of Picachos, north-central Chile. *Ore Geology Reviews*. 112, 103037, https://doi.org/10.1016/j.oregeorev.2019.103037.

Monazzami Bagherzadeh, R., Karimpour, M. H., Farmer, J. L., Stern, C., Santos, J. F., Ribeiro, S., Rahimi, B., and Haidarian Shahri, M. R. (2018-2019): Geochronology, petrology and geochemistry of intermediate and mafic Rocks of the Bornaward plutonic complex (northwest of Bardeskan, Iran). *Journal of Economic Geology*. Vol. 10, No. 2, P: 425–448.

Movahednia, M., Maghfouri, S., Fazli, N., Rastad, E., Ghaderi, M., Gonzalez J.F. (2022). "Metallogeny of Manto-type stratabound Cu-(Ag) mineralization in Iran: Relationship with Neo-Tethyan evolution and implications for future exploration." *Ore Geology Reviews*, 149, 1064.

Niu, S.-D., Li, S.-R., Santosh, M., Zhang, D.-H., Li, Z.-D., Shan, M.-J., Lan, Y.-X., & Gao, D.-R. (2016). Mineralogical and isotopic studies of base metal sulfides from the Jiawula Ag–Pb–Zn deposit, Inner Mongolia, NE China. *Journal of Asian Earth Sciences*. 115, 480–494, https://doi.org/10.1016/j.jseaes.2015.10.020.

Ohmoto, H., & Goldhaber, M.B. (1997). Sulfur and Carbon Isotope: In Barnes, H.L., (ed), Geochemistry of Hydrothermal Ore Deposits, 3rd ed., New York, John Wiley & Sons, p. 517- 611.

Oliveros, V., Feraud, G., Aguirre, L., Ramirez, L., Fornary, M., Palacios, C. and Parada, M. (2008). Detailed 40Ar/39Ar dating of geologic events associated with the Mantos Blancos copper deposit, northern Chile. Mineralium Deposita. 43(2): 281–293, http://dx.doi.org/10.1007/s00126-007-0146-2.

Oyarzum, R., Ortega, L., Sierra, J., Lunar, R. and Oyarzn, J. (1998). Cu, Mn and Ag mineralisation in the Quebrada Marquesa quadrangle, Chile: the Talcuna and Arqueros districts. *Mineralium Deposita* 33: 547- 559.

Palacios, C. (1986). Subvolcanic copper deposits in the Coastal Range of northern Chile. Zentralblatt für Geologie und Pal¨aontologie, Teil I, 1985, H.9/10, Stuttgart. p. 1605–1615, https://doi.org/10.1127/zbl_geol_pal_1/1985/1986/1605.

Pearce, J.A. (1996). A user's guide to basalt discrimination diagrams. In: Trace element geochemistry of volcanic rocks: Applications for massive sulfide exploration (Ed. Wyman, D.A.) Short Course Notes. *Geological Association of Canada*. 12, p79-113.

Pearce, J.A. (1983). Role of the Sub-Continental Lithosphere in Magma Genesis at Active Continental Margins. In: Hawkesworth, C.J. and Norry, M.J., Eds., Continental Basalts and Mantle Xenoliths, Shiva Cheshire, UK, 230-249.

Pirajno, F. (2009). Hydrothermal Mineral Deposits, Principle and Fundamental Concept for the Exploration Geologist». *Springer*, 706 p.

Ramezaniabbakhsh, T., Karimpour, M. H., Azizi, H., Rahimi, B., and Saadat, S. (2023). Metallogeny of mantle-copper deposits, special view in Nasim copper deposit, northwest of Bardaskan, Khorasan Razavi, Iran. *Journal of Economic Geology*, 2023. Vol. 15. No. 1, PP: 143-174, DOI: 10.22067/ECONG.81591.1071.

Rezaeihamid, R., Tale Fazel, A. (2019). Mineralogy, mineralschemistry and sulfur isotope geochemistry of Baharieh copper deposit (NE Kashmar): implications for ore genesis. *Journal of Petrology*, 10 Year. No.39, PP: 53–78.

Rezapanah Khour, H. (2016). Investigation of Geology, Alteration and the Cu Mineralization in Cheshmeh-Hadi Area, Bardaskan (Khorasan Razavi Province, Northeast Iran). Unpublished M.Sc. thesis. Shahid Bahonar University of Kerman, Iran. 148 p. (in Persian with English abstract).

Rice, C. M., McCoyd, R. J., Boyce, A. J., & Marchev, P. (2007). Stable isotope study of the mineralization and alteration in the Madjarovo Pb–Zn district, south-east Bulgaria. *Mineralium Deposita*. 42(7), 691–713, https://doi.org/10.1007/s00126-007-0130-x.

Rollinson, H. (1993). Rising geochemical data: evaluation, presentation, interpretation. Longman John Wiley and Sons, New York, 352 p.

Ruiz, C., Aguilar, A., Egert, E., Espinoza, W., Peebles, F., Quezada, R. and Serrano, M. (1971). Strata-bound copper sulphide deposits of Chile. *Society of Mining Geology of Japan*, 39(2): 252–260, https://doi.org/10.1007/978-3-642-88282-1.

Sato, T. (1984). Manto type copper deposits in Chile: a review. Bull. Geol. Surv. Jpn. 35, 565–582.

Schiano, P., Monzier, M., Eissen, J. P., Martin, H. and Koga, K. T. (2010). Simple mixing as the major control of the evolution of volcanic suites in the Ecuadorian Andes. *Contributions to Mineralogy and Petrology* 160, 297–312, https://doi.org/10.1007/s00410-009-0478-2.

Shafaii Moghadam, H., Hua Li, X., Ling, X.X., Santos, J.F., Stern, R.J., Li, Q.L., Ghorbani, G. (2015). Eocene Kashmar granitoids (NE Iran): Petrogenetic constraints from U-Pb zircon geochronology and isotope geochemistry. Lithos 216–217, 118–135, https://doi.org/10.1016/j.lithos.2014.12.012.

Sheppherd. T.J., Rankin. A.H., Alderton. D.H.M. (1985). A Practical Guide to Fluid Inclusion Studies, Blackie and Son, 239 pp.

Soltani, A. (2016). Mineralogy, geochemistry and genesis of the Abri, Rahbari, and Cheshmeh Marziyeh cu deposit, NW Darooneh. M.Sc. Thesis, Shahrood University of Technology, Iran. 191 p.

Steele-MacInnis, M., Lecumberri-Sanchez, P., Bodnar, R.J. (2012). HokieFlincs_H2O-NaCl: a Microsoft Excel

spreadsheet for interpreting microthermometric data from fluid inclusions based on the PVTX properties of H_2O-NaCl. Comput. Geosci. 49, 334–337, https://doi.org/10.1016/j.cageo.2012.01.022.

Stepanov, A., Mavrogenes, J.A., Meffre, S., Davidson, P. (2014). The key role of mica during igneous concentration of tantalum. *Contributions to Mineralogy and Petrology*. 167, 1009, https://doi.org/10.1007/s00410-014-1009-3.

Sun, S. S., and McDonough, W. F. (1989). Chemical and isotopic systematics of oceanic basalts: implications for mantle composition and processes. *Geological Society, London, Special Publications*, 42(1), 313-345, https://doi.org/10.1144/GSL.SP.1989.042.01.19.

Taefi, N., Mousivand, F., Sadeghian, M. (2014). Mineralogy, geochemistry, and genesis of copper mineralization in the Grik and Gurkhan Southeast of Shahrood. *6 th Symposium of Iranian Society of Economic Geology*, University of Birjand, Birjand, Iran. (in Persian with English abstract).

Tosdal, R.M., Munizaga, F. (2003). Lead sources in Mesozoic and Cenozoic Andean ore deposits, north-central Chile (30–34 ◦ S). Mineral. Deposita. 38, 234–250, https://doi.org/10.1007/s00126-002-0307-2.

Warr, L.N. (2021). IMA-CNMNC mineral symbols. Mineralogical Magazine, 85, 291–320.

Wilkinson, J.J. (2001). Fluid Inclusions in Hydrothermal Ore Deposits. Lithos 55, 229-272, https://doi.org/10.1016/S0024-4937(00)00047-5.

Wilson, N.S.F., Zentilli, M. (1999). The role of organic matter in the genesis of the El Soldado volcanic-hosted manto-type Cu deposit, Chile. *Economic Geology*. 94, 1115–1136, https://doi.org/10.2113/gsecongeo.94.7.1115 .

Wilson, N.S.F. (2000). Organic petrology, chemical composition, and reflectance of pyrobitumen from the El Soldado Cu deposit, Chile. *International Journal of Coal Geology*. 43, 53–82, https://doi.org/10.1016/S0166-5162(99)00054-3.

Wilson, N.S.F., Zentilli, M., Reynolds, P.H. (2003a). Age of mineralization by basinal f luids at the El Soldado manto-type Cu deposit. Chile: 40 feldspar. *Chemical Geology*. 197, 161–176, https://doi.org/10.1016/S0009-2541(02)00350-9.

Wilson, N.S.F., Zentilli, M. (2006). Association of pyrobitumen with copper mineralization from the Uchumi and Talcuna districts, central Chile. *International Journal of Coal Geology*, 65, 158–169, https://doi.org/10.1016/j.coal.04.012.

Wilson, M. (2007). Igneous Petrogenesis. Unwin Hyman, London, 461 p.

Winchester, J. A. and Floyd, P. A. (1977). Geochemical discrimination of different magma series and their differentiation products using immobile elements. *Chemical geology*. 20: 325-343, https://doi.org/10.1016/0009-2541(77)90057-2.

Yilmaz, H., Oyman, T., Nuran Sonmez, F., Arehart, G., Zeki, B. (2010). Intermediate sulfidation epithermal gold-base metal deposits in Tertiary subaerial volcanic rocks, Sahinli/Tespih Dere (Lapseki/Western Turkey), *Ore Geology Reviews*. 37, 236–258, https://doi.org/10.1016/j.oregeorev.2010.04.001.

Zamanian, H., Dolatshahi, S., Yang, X., Karimzadeh S.A,m., Meshkani, S.A. (2021). Geochemical, fluid inclusion and O-H-S isotope constraints on the origin of the Rangraz copper deposit, Central Iran. *Ore Geology Reviews*, Volume 128, January, 103877, https://doi.org/10.1016/j.oregeorev.2020.103877.

Zamanian, H.; Tale Fazel, E.; Sameti, M.; Asadi Haroni, H.; Yang, X. (2023). The petrogenesis and metallogenesis of the Kalchuyeh epithermal gold deposit, central Iran: Constraints from geochemistry, fluid inclusion, and H–O–S isotopes. *Journal of Asian Earth Sciences*, Article 105505, DOI: 10.1016/j.jseaes.2022.105505.

Zentilli, M., Collins, P.G., Boric, P.R., Wilson, N. F. S. (2009). Diagenetic pyrite in the El Soldado stratabound copper deposit: a link with the petroleum system of the Cretaceous basin of central Chile. XII Congreso Geologico Chileno Santiago.

Zentilli, M., Munizaga, F., Graves, M.C., Boric, R., Wilson, N.S.F., Mukhopadhyay, P.K., Snowdon, L.R. (1997). Hydrocarbon involvement in the genesis of ore deposits: an example in Cretaceous strata-bound (manto-type) copper deposits of central Chile. *International Geology Review*. 39, 1–21, https://doi.org/10.1080/00206819709465257.

Zhang, Y.G., Frantz, J.D. (1987). Determination of the homogenisation temperatures and densities of superficial fluids in the system NaCl-KCl-$CaCl_2$-H_2O using synthetic fluids inclusions. *Chemical geology*. 64, 335–345, https://doi.org/10.1016/0009-2541 (87)90012-X.

Zheng, Y. F. (1993b). Calculation of oxygen isotope fractionation in hydroxyl-bearing silicates. *Earth and Planetary Science Letters*. 120, pp. 247-263, https://doi.org/10.1016/0012-821X(93)90243-3.

SAŽETAK

Rudna geneza i hidrotermalna evolucija slojevitoga (tipa Manto) ležišta bakra Cheshmeh-Hadi u vulkansko-plutonskome pojasu sjeverno od rasjeda Doruneh, istočno od ležišta bakra Sepid-Sarve (sjeverozapadni Bardeskan, središnji Iran): dokazi iz geologije, geokemije, fluidnih inkluzija i stabilnih izotopa S i O

Ležište bakra Cheshmeh-Hadi dio je eocenskoga vulkansko-sedimentnog slijeda smještenoga u južnoj zoni Sabzevar. Litostratigrafski slijed, od najstarijeg do najmlađeg, obuhvaća bazalt, bazaltni andezit, andezit i piroksenski andezit, konglomerat, vapnenac, siltit, gipsoviti lapor i pliocenski konglomerat. Mineralizirana zona javlja se unutar konglomerata i na kontaktu između konglomerata i andezita. Tipični rudni minerali jesu malahit-azurit, halkocit, bornit, kovelit i povremeno samorodni bakar. Povezani hidrotermalni fluidi upućuju na umjeren do visok salinitet, u rasponu od 3,09 do 13,39 težinskih % ekvivalenta NaCl, s temperaturama homogenizacije između 89 i 387 °C, što upućuje na miješanje fluida tijekom stvaranja rude. Halkocit rijetko prati kvarc, što sugerira nizak sadržaj silicija u fluidima koji stvaraju rudu. Vrijednosti $\delta^{34}S$ uzoraka sulfida iz proučavanoga ležišta kreću se od –24,1 ‰ do –2,6 ‰, dok se vrijednosti $\delta^{34}S$ hidrotermalnog H_2S kreću od –24,3 ‰ do –2,6 ‰. Vrijednosti $\delta^{18}O$ hidrotermalnih fluida povezanih s mineralizacijom spadaju u raspon bazaltnih stijena, meteorskih voda i sedimentnih stijena. Geokemijske varijacije glavnih i elemenata u tragovima upućuju na kontaminaciju kontinentalne kore u magmatskoj evoluciji. Istraživane vulkanske stijene spadaju u kalcijsko-alkalna do šošonitna polja, formirana u okruženju kontinentalnoga luka, a koja potječu iz obogaćenoga izvora plašta pod utjecajem fluida povezanih sa subdukcijom. Ove stijene karakterizira osiromašenje HREE-a, umjereno obogaćivanje LREE-a i slaba negativna Eu anomalija. Na temelju rezultata istraživanja ležište Cheshmeh-Hadi klasificirano je kao stratificirano ležište bakrenoga sulfida, nastalo u vulkansko-sedimentarnome okruženju povezanom s magmatskim lukom pod utjecajem subdukcije.

Ključne riječi:
Cheshmeh-Hadi, slojevito vezani bakar, vulkansko-plutonski pojas, stabilni izotopi, središnji Iran

Authors contribution

Morteza Esform (PhD student, Department of Geology at Lorestan University, Khorramabad): conceptualization, data curation, formal analysis, investigation, methodology, project administration, resources, software, supervision, validation, visualization, writing – original draft and writing – review & editing. **Hasan Zamanian** (Full professor of geology, School of Geology, College of Science, University of Tehran): project administration, methodology, review & editing. **Alireza Zarasvandi** (Full professor, Department of Geology, Faculty of Earth Sciences, Shahid Chamran University of Ahvaz): resources. **Alireza Almasi** (PhD, Department of Geology, Faculty of Science, Lorestan University, Khorramabad): resources. **Mahya Manouchehry Nia** (Department of Geology, Faculty of Science, Lorestan University, Khorramabad): resources.
All authors have read and agreed to the published version of the manuscript.